Self-polymerized Dopamine Thin Film as Bioadhesive

by

Fut Yang

A thesis
presented to the University of Waterloo
in fulfillment of the
thesis requirement for the degree of
Master of Applied Science
in
Chemical Engineering

Waterloo, Ontario, Canada, 2011

AUTHOR'S DECLARATION

I hereby declare that I am the sole author of this thesis. This is a true copy of the thesis, including any required final revisions, as accepted by my examiners.

I understand that my thesis may be made electronically available to the public.

Abstract

Dopamine is an interesting biomolecule that functions as a neurotransmitter in the brain. It has been found able to stick to almost all surfaces due to its unique catecholamine structure. Under alkaline conditions, the catechol functional group oxidizes to quinone allowing dopamine to self-polymerize and form thin films on support surfaces. The facts that dopamine can be coated to virtually any materials and the amine and catechol functional groups support a variety of reactions with organic species make polydopamine an attractive multifunctional bioadhesive/coating. To date, most of research on polydopamine has been focusing on its applications as thin films and little attention has been paid to the adhesion aspect of the material.

In the study, we evaluated the properties of self-polymerized dopamine thin films as a bioadhesive. The thesis consists of three consecutive studies: (i) characterization of the adhesion properties of polydopamine thin films; (ii) investigation of the mechanical properties of polydopamine thin films; and (iii) exploration of the potential of polydopamine thin films as a wet adhesive. Fundamental insights on the wettability, adhesion behaviours, and mechanical properties of polydopamine thin films for both wet and dry conditions were derived through sets of well-designed contact angle, contact adhesion, and contact deformation experiments. It was found that dopamine is able to coat plastic, ceramic and metal surfaces, and join or bond rigid substrates but might not be suitable for joining soft or flexible parts as polydopamine is fairly rigid and the bonding might be too slow and too rigid for practical applications if polydopamine is directly used as an adhesive. Based on the understanding, a new strategy for fabricating underwater adhesive was proposed and tested. In the strategy, polydopamine with ferric ion as the oxidant was utilized as a cross-linker to alginate solution, effectively turning the solution into a wet adhesive, which demonstrated better practical performances than other studies; the adhesive was able to produce a permanent tensile adhesive strength of 80 kPa joining aluminum and glass with macroscopic roughness at the interface within 2 hours of curing time.

Inspired by the results from the contact deformation experiments, we were able to extend the JKR theory with the well-known plate theory to accommodate the deformation of nanometer thin films, obtaining their elasticity. We termed this extended theory the “thin film contact mechanics” and validated the theory against gold thin films and found it predicted the mechanical behaviours of the thin films fairly well.

Acknowledgements

I would like to express my sincere gratitude to my supervisor, Dr. Boxin Zhao, for his continuous support of my Master's study and research, for his patience, motivation, enthusiasm, and immense knowledge. His guidance encouraged and helped me in all the time throughout the entire process of my program. I would like to thank him not only as a mentor in research but also as a role model who showed great character in dealing with challenges and handling problems. I could not have imagined having a better advisor and mentor for my study. What he did for me is beyond my expectations and will continue to inspire me in my career and life in future.

Beside my supervisor, my thanks also go to my colleagues. I would like to thank Yougun Han for his tireless hard work on the hardware and software of the micro-indentation and the contact angle measurement systems. Without him, it would be impossible for me to proceed in research. I would like to thank Hadi Izadi for providing valuable advices and stimulating scientific discussions. Also, I would like to thank Daniel Cho for all the fun we had during his internship here. The list would not be complete without thanking the rest of my colleagues for making a cheerful working environment.

Finally, I would like to express my thanks to my parents, Kuen Kuen Tsui and Mian Yun Yang, for giving birth to me and supporting me spiritually throughout my life.

Table of Contents

List of Figures

List of Tables

Chapter 1
Introduction

Advances in adhesive technology over the last century have led to the widespread replacement of joining technologies such as mechanical fastening, soldering, and wire bonding with adhesive bonds in everything extending from sticking a note to the construction of modern aircrafts [1]. The appeal of adhesives is compelling because adhesives have the ability to join similar or dissimilar material components, allow better load distribution in joints, provide better design flexibility, and ultimately lead to improved cost effectiveness [2]. In recent years, there has been increasing interest in biological alternatives to synthetic adhesives due to rising oil prices, environmental concerns, and health and safety issues [3]. Bioadhesives are of commercial interest because they tend to be hydrophilic and biocompatible, which are useful for biomedical and underwater applications.

Much of the research of bioadhesives was motivated and inspired by the discoveries and phenomena found in nature. In the sea, there is a diversity of organisms that specialize in sticking to all type of wet surfaces: mussels hang on with a handful of threads constructed to alleviate the mechanical mismatch between hard rock and soft invertebrate body [4], barnacles glue calcareous base plates to rocks and boat bottoms [5], and sandcastle worms live in tubes composed of sand, shell fragments, and blobs of underwater proteinaceous glue [6]. Through the study of amino acid composition of proteins [7], DOPA (3,4-dihydroxy-L-phenyalanine), an amino acid formed by posttranslational modification of tyrosine, had been identified as a recurrent constituent of the glues from these organisms. In particular, the catechol functionality of DOPA is mainly responsible for water-resistant adhesion and that the o-quinone functionality (oxidized catechol) is primarily responsible for cross-linking of the glues [8]. Although the exact binding mechanism of catechol functionality to different materials is still not fully understood, it has been reported from a single-molecule study of DOPA [9] by atomic force microscopy that as revealed by the magnitude of the bond dissociation energy, the binding mechanism is not hydrogen bond formation and the oxidation of DOPA reduces the strength of interactions to metal oxide but results in the formation of high strength irreversible covalent bond to an organic surface. Evidences suggested that the interactions is co-ordination bonding with metal or metal oxide which involves the replacement of a surface hydroxyl group with deprotonated ligand [10-12] and the interactions is covalent with organic surfaces via Michael addition and Schiff base reactions [13, 14]. Due to its broad reactivity, catechol functionality has become the center of bioadhesive research leading to some interesting developments in the field. For instance, a reversible

wet/dry adhesive surface, geckel, by conjugating catechol functionality to a gecko patterned surface [15].

The most fascinating advance in field for us is the use of dopamine as a coating material pioneered by Lee *et al* [16]. Dopamine is an interesting biomolecule that functions as a neurotransmitter in the brain and is responsible for human motivation and pleasure [17]. It has a chemical structure of catecholamine mimicking the chemical composition of mussel adhesive proteins of which the proteins contain unusually high concentrations of catechol and amine functional groups. Under alkaline conditions, the catechol functional group oxidizes to quinone allowing dopamine to self-polymerize and form thin films on support surfaces. Although the exact mechanism is unknown, the polymerization process likely proceeds in a manner reminiscent of melanin formation [18]. The chemical composition and optical properties of polydopamine, characterized by a broadband absorption spectrum over the UV-visible range of the electromagnetic spectrum and by X-ray photoelectron spectroscopy, are consistent with those of melanin [19-21]. Reactivity similarities with melanin were also observed in the investigation of spontaneous oxidation of dopamine in the presence of dissolved dioxygen or other oxidants [22]. The thickness of the polydopamine film can be controlled with a rate of growth proportional to the reaction time if fresh dopamine is regularly provided [19] and the deposition kinetics of the film can be markedly modified using different oxidants such as oxygen, ammonium persulfate, and metal ions [23]. The facts that polydopamine can self-polymerize and coat to virtually any materials and its amine and catechol functional groups can support a variety of reactions make polydopamine an attractive multifunctional bioadhesive/coating. To date, most of research on polydopamine has been focusing on the application of polydopamine thin films, very little attentions have been paid to the adhesion and mechanical aspects of polydopamine, and let alone the potential application of polydopamine as a wet adhesive.

This thesis comprises three consecutive studies performed in my Master's study: (i) characterization of the adhesion properties of polydopamine thin films in dry conditions to derive fundamental insights into the wettability and the adhesion behaviour of polydopamine; (ii) investigation of the mechanical properties of polydopamine thin films through contact deformation studies to comprehend its performances as a joint; and (iii) exploration of the application of polydopamine as a wet adhesive in which the characterization of the adhesion properties of polydopamine is extended to wet conditions and attempts are made to combine polydopamine with hydrogel to form a practical wet adhesive. It is organized into six chapters and the research chapters 2-5 are written in the format of

journal manuscripts. The first study is described in Chapter 2 where the result provide us with not only a better understanding on the surface behaviour and adhesion properties of the thin films, but also effective strategies for exploiting properties of dopamine to create novel applications. Chapter 3 describes the contact deformation behaviours of polydopamine thin films by micro-indentations in the framework of JKR (Johnson, Kendall, and Roberts) contact mechanics. In the study, we were able to extend the JKR theory to accommodate the deformation of nanometer thin films, obtaining their elasticity. We term this extended theory the "thin film contact mechanics" and a detailed derivation of the theory is provided in Chapter 4. The theory is validated against gold thin films and its applicability is discussed and compared with nano-indentation. Chapter 5 presents the third study in regards to the wet adhesion aspect of polydopamine. Polydopamine is characterized in wet conditions and a new strategy for fabricating underwater adhesive is proposed and tested. In the strategy, polydopamine is utilized as a cross-linker to alginate solution, effectively turning the solution into a wet adhesive. The performance of the adhesive is discussed and compared to other studies that employ different strategies.

Chapter 2
Adhesion Properties of Self-polymerized Dopamine Thin Film

2.1 Introduction

As future technological innovations gear toward miniaturizing machines and maximizing performance density, effective joining of similar or dissimilar material components has become one of the most critical technical prerequisites for manufacturing at ever smaller scales. Compared to soldering and wire bonding technologies, adhesive bonding offers numerous advantages such as environmental friendliness (elimination of lead and flux cleaning), mild processing conditions, fewer processing steps, and especially, the fine pitch capability to make microjoining possible due to the availability of small size conductive fillers. However, the performance of adhesive bonding depends significantly on the quality of surfaces. Surface pre-treatments are commonly required for the success of adhesive bonding. In this article, we report an experimental study of the surface and material properties of the self-polymerized polydopamine thin film and discuss its potential application as a novel coating and adhesive material.

Dopamine, commonly known as a neurotransmitter, is a small molecule mimic of the adhesive component, L-DOPA, of marine mussels with the chemical structure of catecholamine. Under alkaline conditions, the catechol functional group oxidizes to quinone allowing dopamine to self-polymerize and form a thin film on support surfaces through covalent bond and other strong intermolecular interactions such as hydrogen-bonding, metal chelation, and π-π interactions [9, 16]. In 2007, Lee and coworkers reported the method of dip-coating objects in an aqueous solution of dopamine and found a nanometer thin layer of polydopamine formed on a wide range of different substrates including noble metals, oxides, semiconductors, ceramics, and synthetic polymers [16, 24 25]. They also demonstrated polydopamine coating as a universal route for material functionalization for such applications as improving wet adhesion, conjugating organic components, and supporting spontaneous electroless metal depositions. Lee's work has led to continuously increasing research activities on polydopamine coatings in various fields including biosensors and bioelectronics [26-29], tissue and pharmaceutical engineering [30-33], nanotechnology [34-38], and membrane science [39-45]. Recently, Ryu and coworkers reported dopamine coating as a universal route to produce robust organic-inorganic biocomposites by bio-mineralization of hydroxyapatite on polydopamine thin films [46]. Xing and Yin reported that polydopamine is a suitable adhesive for assembling halloysite

nanotubes on electrodes [47]. Xu and coworkers reported the dopamine-induced reduction and functionalization of graphene oxide nanosheets for subsequent grafting of polymer brushes [48]. Bernsmann and coworkers characterized the dopamine-melanin growth on silicon oxide and found that the thickness of these coatings can be controlled to allow a growth regime that is proportional to reaction time [19, 43].

In this study, we hypothesize that dopamine aqueous solutions can be used as adhesives since dopamine adsorbs on almost all kinds of surfaces, in particular on metal surfaces by forming strong coordination bonds [9, 49], and develops cohesive strength through self-polymerization [50]. To the authors' best knowledge, there have been no systematic studies of the adhesion and associated micromechanical properties of polydopamine thin films. The research works reported in the article are the first steps toward elucidating the adhesion behaviour of polydopamine. Three types of experimental studies (water contact angle, contact adhesion, and adhesive bonding) were described and discussed to derive fundamental insights into the wettability and adhesion behaviour of polydopamine thin films coated on or bonded between metal and glass or polymer substrates.

2.2 Materials and Experimental

Dopamine hydrochloride was supplied by Sigma-Aldrich. TRIS-HCl buffer base (BP152) was supplied by Fisher BioReagents. Polydimethylsiloxane (PDMS, Sylgard 184) was supplied by Dow Corning Corp., Midland, MI. Aluminum SEM studs (Product No: 16111) were supplied by TED PELLA, INC. Plain microscope slides were supplied by Fisher Scientific. Microscope slides and aluminum stools were cleaned by acetone and deionized water before use. The experimental setup is illustrated in Figure 2.1 and described below.

2.2.1 Preparation of Flat Sheets and Hemispherical Tips of PDMS

PDMS solution used for making elastomers was prepared by mixing the elastomer base and crosslinker at a weight ratio of 10:1. The flat sheet of PDMS was made by casting 2 ml of PDMS solution onto a microscope slide and curing at 90 °C for 1.5 hours in ambient air. The sheet thickness was measured to be 1.25 ± 0.1 mm. The hemispherical tip of PDMS was made by first molding the PDMS solution into a hemispherical shape using a custom-made Teflon mold and then coating the resulting PDMS tip with a layer of PDMS solution to make the tip surface smooth. The tip core was cured at 90 °C for 15 min and the tip coating along with the core was then cured at 90 °C for 1.5

hours in ambient air. The resulting tip radius was measured to be 2.8 ± 0.1 mm by analyzing the side-view image of the tip using a custom-written MATLAB (R2008a, MathWorks) script which gives a least squares best-fit to the curvature of the apex of the tip.

2.2.2 Coating Polydopamine Thin Films on PDMS Elastomers

The dopamine solution used for coating was made by dissolving dopamine hydrochloride at a concentration of 2 mg/ml in a 10 mM TRIS-HCl buffer at pH 8.5. PDMS elastomers were submerged in the dopamine solution immediately for a period of 24 hours once the solution was made. To avoid the deposition of polydopamine nanoparticles formed in the solution during the coating process, all samples of PDMS elastomers were placed upside down in the solution. The coated samples were air dried overnight. The surface quality of the coatings was examined by optical microscope (Omano OMM300T) and Veeco Optical Profiling System (WYKO NT1100).

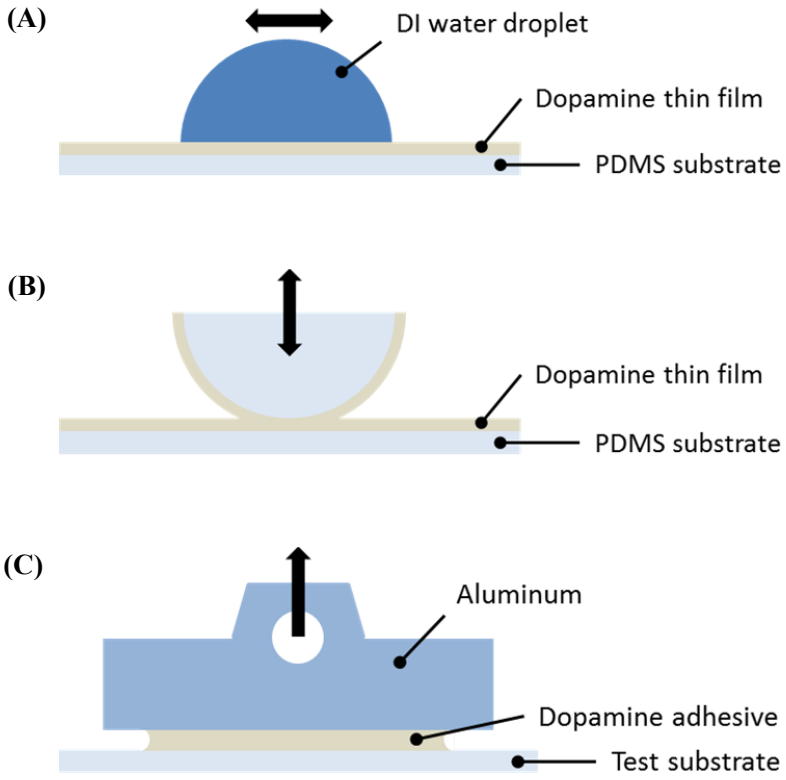

Figure 2.1: Schematics of three characterization techniques: (A) contact angle measurement, (B) contact adhesion test, and (C) pull-off bonding test. Black arrows represent the direction of movements.

2.2.3 Contact Angle Measurements of Polydopamine Thin Films

The sessile drop method was used to determine the wettability of deionized water on surfaces coated in 2 mg/ml dopamine solution for 24 hours, as shown in Figure 2.1A. A drop of 5 µl was dispensed onto the polydopamine-coated surface from a height of 2 cm to determine the static contact angle. After that, the needle was brought down into the drop from the top center. Advancing and receding contact angles were measured by increasing 10 µl (growing phase) and then decreasing 15 µl (contracting phase) of the drop volume at a rate of 100 µl/min to ensure that the three phase boundary line moves over the surface. A period of 20 sec, called the relaxing phase, was waited between the growing phase and the contracting phase. The images of the drop were recorded and analyzed by a custom-developed LabVIEW (version 8.5, National Instruments) program in terms of contact angle, drop volume, and drop contact radius as a function of time. All measurements were performed in ambient air at the room temperature.

2.2.4 Contact Adhesion of Polydopamine Thin Films

Contact adhesion measurements were carried out using a custom-made micro-indentation system that is comprised of a linear stage (Newport MFA-CC), a 25 g force transducer (Transducer Techniques GS0-25), and an inverted optical microscope (Omano OMM300T) and controlled by a custom-developed LabVIEW (version 8.5, National Instruments) program. Hemispherical PDMS tips were brought into contact with flat sheets of PDMS coated on glass, as shown in Figure 2.1B, at a speed of 0.1 µm/sec until a preload force of 5 mN was detected, held in contact at the preload for 5 min, and then separated at the same speed. Three sets of tests, uncoated PDMS tip on PDMS substrate (PDMS-PDMS), PDMS tip on polydopamine-coated PDMS substrate (PDMS-PDMS(D)), and polydopamine-coated PDMS tip on polydopamine-coated PDMS substrate (PDMS(D)-PDMS(D)), were conducted at the room temperature under dry conditions. Force, displacement, and time information were recorded.

2.2.5 Pull-off Tests of Dopamine Adhesive Bonds/Joints

Pull-off tests of aluminum studs joined by dopamine aqueous solutions on glass and PDMS substrates were performed to determine the adhesive bonding strength of polydopamine. PDMS substrates were pre-coated with dopamine solution at 2 mg/ml for 1 hour to reduce surface hydrophobicity. Aluminum studs, 4 g in weight and 12.7 mm in base diameter, were placed on top of the substrates with 2 µl of dopamine solution in between, as shown in Figure 2.1C. The joints were placed in

ambient air at the room temperature for 1 hour then at 90 °C for 1 hour to allow dopamine to polymerize and dry before testing. The bond strength was determined using a Texture Analyzer (Texture Technologies Corp. TA.XT.plus) at a speed of 0.1 mm/sec.

2.3 Results and Discussion

2.3.1 Wettability Characterization

Good wetting of adhesives on substrate surfaces is the prerequisite for successful bonding or joining. The wettability of polydopamine-coated PDMS surfaces was investigated by water contact angle measurements. The static contact angle of deionized water drop on polydopamine-coated PDMS surface was measured to be 65°, revealing the hydrophilic nature of self-polymerized dopamine films. This static contact angle is consistent with the value reported in literature [32] suggesting the PDMS substrate was completely covered by a layer of polydopamine. Note that the PDMS surface is hydrophobic, having a water contact of 105°. To obtain further insights on the properties of polydopamine-coated surface, we designed and performed dynamic contact angle measurements by continuously enlarging and subsequently reducing the size of water drop through an embedded needle. Figure 2.2A shows typical optical images of initial, advancing, and receding water drops for static and dynamic contact angle measurements. Figure 2.2B plots the contact angle, volume, and radius of the contact area of the drop on the surface as a function of time. We noticed that the initial contact angle in the dynamic measurement was same as the static contact angle, suggesting a negligible effect of the embedded needle on contact angle. The contact angle of the drop in the growing state that reached a steady-state value after 7 sec is defined as the advancing contact angle θ_a, which is about 5° higher than the static one. There was a slight delay between the volume increase and the area increase, called the contact line "pinning" effect [51]. As the drop stopped growing, the contact angle relaxed and remained constant at an angle slightly higher (~4°) than the initial angle, perhaps due to the increase of volume and the pinning effect. In the contracting region, a more significant contact line "pinning" effect was observed; this effect caused the contact angle to decrease with the volume while the radius remained constant. The lowest contact angle, occurred at the moment the contact line started to move, is defined as the receding contact angle θ_r, which is 10°. The contact angle hysteresis, i.e. $\theta_a - \theta_r$ was determined to be 60°. The low receding angle and large hysteresis suggested the formation of a hydration layer or bound water layer upon contacting with water. This is reasonable considering the amine and hydroxyl groups of dopamine are capable to

reorient and form hydrogen bonds with water molecules. Thus, we suspect that the surface of polydopamine coating layer had not been completely polymerized; a large amount of free amine and hydroxyl groups existed at the surface.

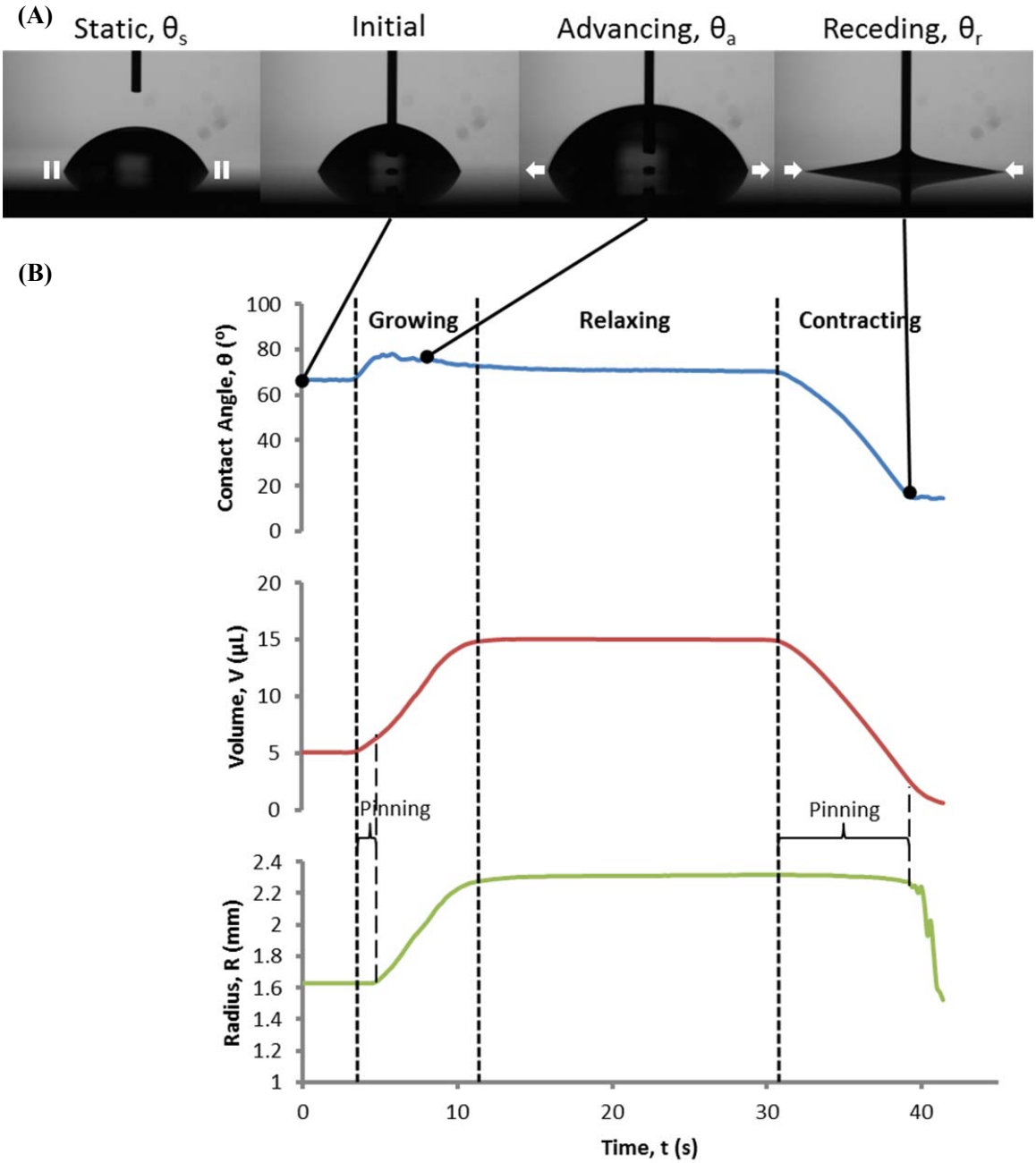

Figure 2.2: Wettability Characterization: (A) typical optical images of static and dynamic contact angles and (B) plots of contact angle, drop volume and drop contact radius vs. time.

2.3.2 Contact Adhesion Properties of Polydopamine-coated Surfaces

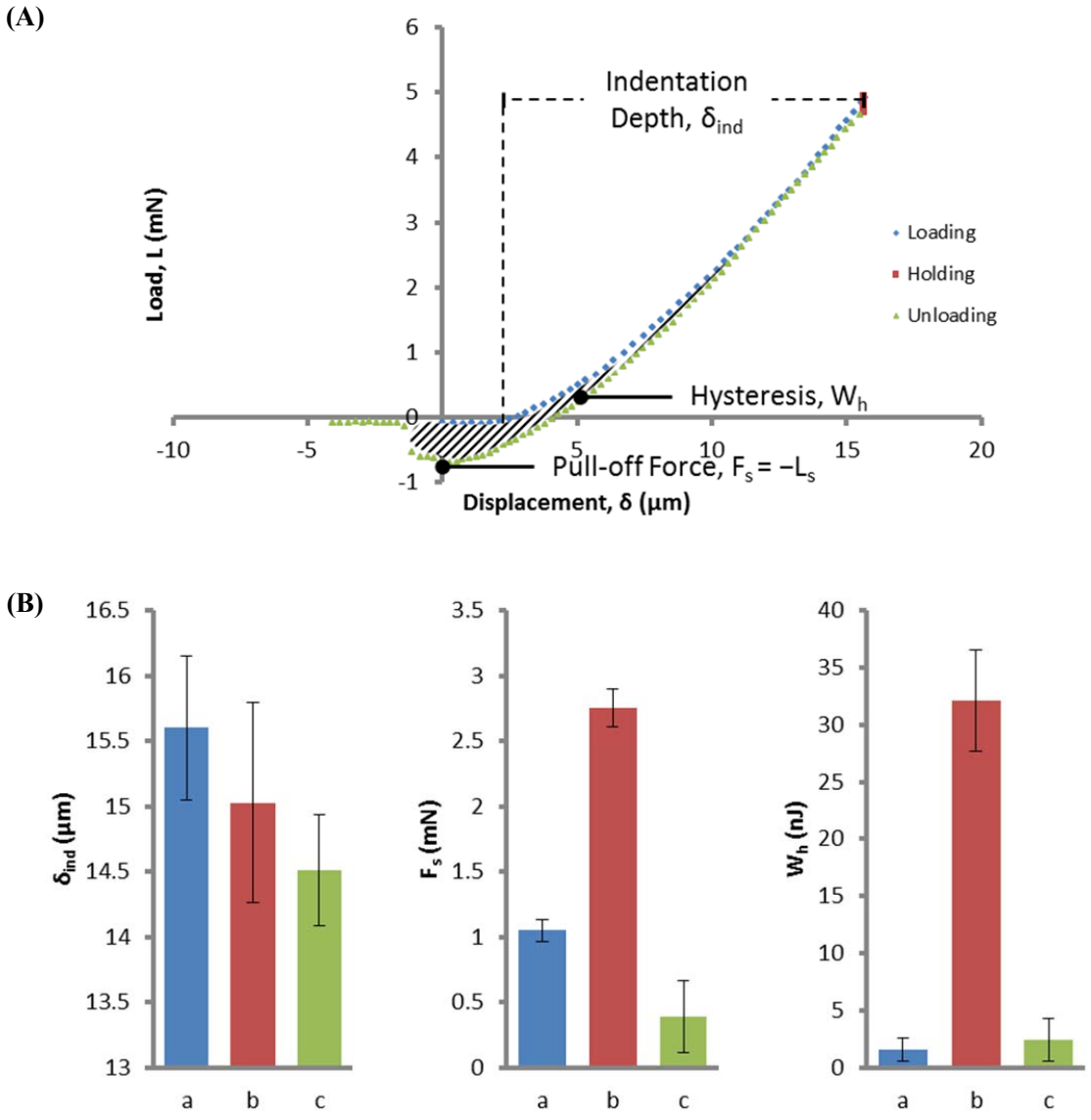

Figure 2.3: Contact Adhesion Properties of Polydopamine-coated Surfaces: (A) typical load vs. displacement curve and three characteristic parameters: indentation depth δ_{ind}, pull-off force F_s, and hysteresis W_h , and (B) comparison of the three parameters for the contacts between (a) PDMS and PDMS, (b) PDMS and PDMS(D), and (c) PDMS(D) and PDMS(D).

The adhesion properties of polydopamine thin films were studied in terms of self-adhesion and adhesion to PDMS surfaces. Figure 2.3A shows a typical force vs. displacement curve for the contact adhesion between two polydopamine-coated surfaces, characterized by a negative tensile force and a loading-unloading hysteresis. The surface force induced "jump-in" phenomenon was not observed in the self-adhesion tests suggesting that either the surface was rigid or rough. For quantitative analyses, we defined three characteristic parameters extracted from the force vs. displacement curves: (a) the pull-off or separation force called the adhesive force $F_s = -L_s$, (b) the adhesion hysteresis W_h (i.e. the energy loss during the loading-unloading cycles), and (c) the indentation depth or displacement δ_{ind} at the applied preload, which is related to surface compliance.

Figure 2.3B is a comparison of these three parameters obtained from the indentation tests between (a) two bare PDMS surfaces as a control, (b) polydopamine-coated and PDMS surfaces, and (c) two polydopamine-coated surfaces. The indentation depth δ_{ind} declined consistently in the order of PDMS-PDMS, PDMS-PDMS(D), and PDMS(D)-PDMS(D) suggesting the polydopamine thin film is more rigid than the PDMS surface. As for the adhesive force F_s, the asymmetric contacts between PDMS and PDMS (D) have the highest value while the contacts between PDMS (D) and PDMS (D) have the lowest value. The comparison in the hysteresis parameter shows a much more pronounced difference between the asymmetric contacts and the other two symmetric contacts. It is interesting to notice that the polydopamine surface seemed inert to itself but active to the PDMS surface. We suspect that there might be specific interactions between polydopamine and PDMS considering that some amine and hydroxyl groups on the former surface that might not be polymerized (as revealed from the large contact angle hysteresis) and are able to actively interact with the latter surface. The reason for the observed low self-adhesion of polydopamine-coated surface is not known. Ongoing in-depth characterizations of the polydopamine coating in term of surface composition and topography will be able to reveal more insights into this observation.

2.3.3 Dopamine Adhesive Bonding

The adhesive bonding behaviour and as well as the practicality of joining with dopamine solutions of different concentrations were investigated by using the solutions to join aluminum studs to two different flat substrates: hydrophilic glass and hydrophobic PDMS elastomer. We noticed that the dopamine solution could not directly be used to join the Al and PDMS because PDMS is hydrophobic and the solution was squeezed out during bonding. We found a pre-treatment of PDMS with

dopamine necessary for a successful bonding process. As shown in the wettability studies, the surface of PDMS can be changed from hydrophobic to hydrophilic after coating with a thin layer of polydopamine. We utilized this finding and brought the contact angle of PDMS down to 95° with 1 hour of pre-treatment to avoid the squeeze-out of dopamine solutions. The bonded areas were examined under an optical microscope; circular shapes were observed with a diameter of 5 mm for Al/glass and 10 mm for Al/PDMS.

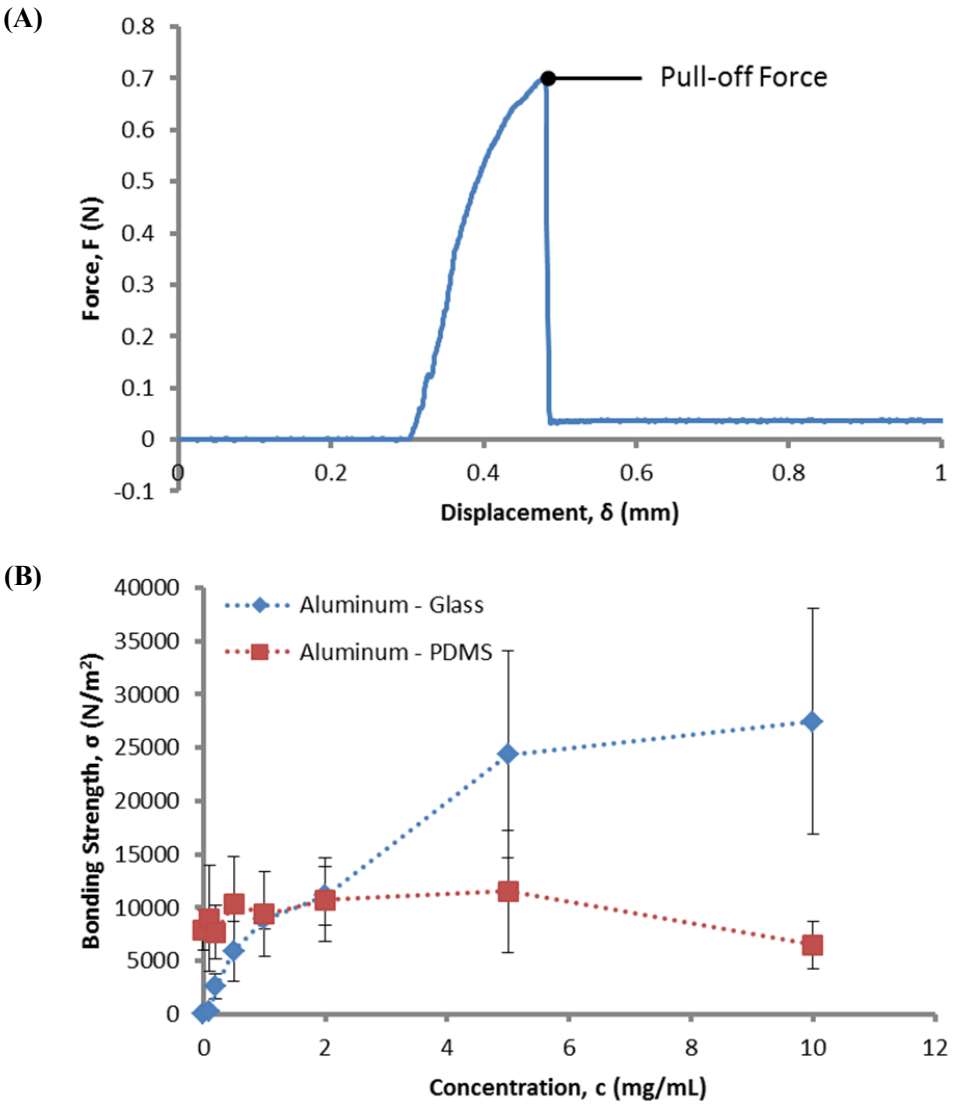

Figure 2.4: Dopamine Adhesive Bonding: (A) typical force displacement curve for the pull-off measurement and (B) plot of adhesive bonding strength vs. dopamine concentrations.

Figure 2.4A shows the typical force vs. displacement curve when pulling bonded substrates apart in tensile mode. The maximum force, called the pull-off force, is normalized by the bonded area to give the adhesive bonding strength in N/m^2. The detached surfaces were examined under an optical microscope showing remains of dopamine adhesive on both surfaces. Thus, the failure of adhesive bonds happened mostly within the polydopamine layer revealing that the bonds formed between dopamine and its substrate surface is strong. This is consistent with the observation of the low self-adhesion of polydopamine surfaces. Figure 2.4B shows the bonding strength as a function of dopamine concentrations on glass and on PDMS substrate. It can be seen that the dopamine bonding of PDMS and Al is significantly different from that of glass and Al. There was no adhesion between bare Al and glass; the adhesive strength increased with dopamine concentration and levelled off at a concentration of 5 mg/ml or a surface coverage of 0.51 g/m^2. For the combination of PDMS and Al, there was a finite adhesion between the bare surfaces; adding dopamine has a negligible effect on the adhesive strength at low concentrations but a detrimental effect when the concentration is above 5 mg/ml or a surface coverage of 0.13 g/m^2.

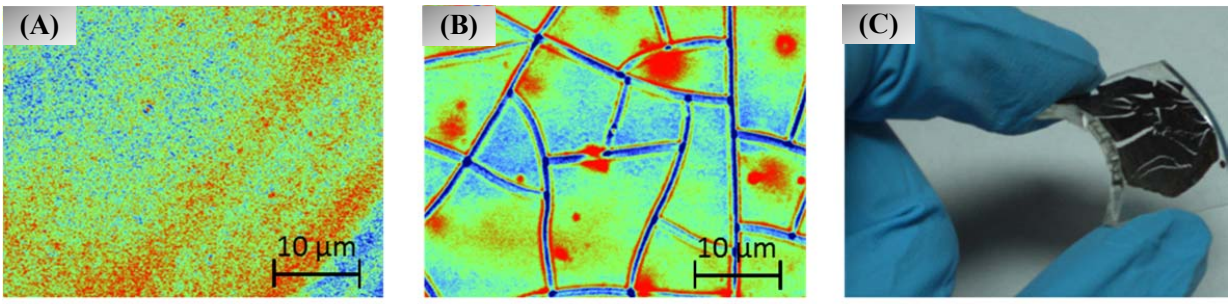

Figure 2.5: Optical images of (A) polydopamine-coated glass surface, (B) polydopamine-coated PDMS surface by Veeco optical profiling system, and (C) bent polydopamine-coated PDMS.

To acquire further insights into the adhesive bonding of the polydopamine layer, we carefully examined polydopamine-coated surfaces using the Veeco Optical Profiling System. Figure 2.5 shows typical images: no cracks were seen on the polydopamine-coated glass surface (Figure 2.5A), but numerous micron-sized cracks were seen on the polydopamine-coated PDMS surface (Figure 2.5B). Furthermore, when we coated a thick layer of polydopamine on PDMS and slightly bent it, we found visible macron-sized cracks formed on the coating which partly delaminated the coating from the substrate (Figure 2.5C). The cracks revealed the brittle nature of the dry polydopamine film. Mismatch of the elastic modulus between the rigid polydopamine film and its soft substrate might be the reason of forming cracks, rendering the polydopamine bonding of PDMS and Al ineffective. We

may conclude that the brittle nature of polydopamine thin film limits its cohesive strength which in turn limits the overall bonding strength.

2.4 Conclusions

Three types of experimental studies (water contact angle, contact adhesion, and adhesive bonding) had been performed to investigate the adhesion behaviour of polydopamine thin films coated on or bonded between inorganic and polymer substrates. Polydopamine-coated polydimethylsiloxane surface had a static contact angle of 65°, suggesting a complete surface coverage by a layer of polydopamine. Wettability of the polydopamine-coated surface was further characterized by dynamic water contact angle measurements, revealing a large contact angle hysteresis of about 60° between the advancing and receding angles. The low receding contact angle suggested the formation of a hydration layer when exposed to water. Polydopamine-coated surfaces in air are relatively inert and have a low self-adhesion compared with the uncoated PDMS surfaces, reflecting the non-conformal, glassy nature of the polydopamine layer. The asymmetric contact between the polydopamine-coated surface and PDMS surface showed the highest adhesion force and hysteresis. The dopamine solutions was found able to bond two rigid surfaces (Al and glass) and the adhesive bonding strength increased with the amount of dopamine and saturated at 5 mg/ml. The direct joining of Al and PDMS using dopamine solution was challenging because of the hydrophobic nature of PDMS; a pre-coating of dopamine on PDMS was found useful. There were no significant bonding strength enhancements in the PDMS/Al system. In summary, the present study in elucidating the surface and adhesion behaviour of polydopamine revealed that dopamine is able to coat plastic, ceramic and metal surfaces, and join or bond rigid substrates but might not be suitable for joining soft or flexible parts as polydopamine films are glassy.

Chapter 3
Mechanical Properties of Self-polymerized Dopamine Thin Film

3.1 Introduction

Films and coatings bonded to substrates often develop in-plane tensile stresses or residual stresses, σ, large enough to cause cracking. In the previous study, numerous micron-sized cracks were seen on the polydopamine coated PDMS surface. These cracks can significantly weaken the integrity of polydopamine and therefore reduce its application's performance, i.e. limiting the overall bonding strength of polydopamine in dry conditions as shown in Chapter 2. Considering that the polydopamine thin films have been studied to improve substrate surface's hydrophilicity and biocompatibility [32], to serve as a nanometer thin ad-layer for electroless metallization on non-metal substrates [28], and to imprint peptides, proteins and DNA/RNA for bio-sensing [29], it is important and essential to understand the mechanical behaviours and the cracking characteristics of polydopamine thin films, in particular, under external stress/strain fields, in order to transfer them effectively into practical applications.

Crack propagation in a film bonded to a substrate is a three-dimensional process, as shown in Figure 3.1, where the crack initiates at a flaw and advances by channelling. This process has been modeled by Beuth [52]. For a fully cracked film of thickness, h, where the depth of the crack reached the film-substrate interface and the crack faces are subject to uniform pressure loading, σ, the change in elastic energy, ΔE, per unit depth in the system due to the introduction of the crack is:

$$\Delta E = \frac{\sigma}{2}\int_0^h \delta(z)dz \qquad \text{Eq. 3.1}$$

where $\delta(z)$ is the crack opening displacement. At steady state, by considering the energy difference between sections of the film (f) /substrate (sub) system far ahead and far behind the crack front, the energy release rate due to channelling of the crack is

$$G_{ss} = \frac{\sigma^2 h}{2E_f^*}\pi g(\alpha,\beta) \qquad \text{Eq. 3.2}$$

α and β are Dundurs parameters:

$$\alpha = \frac{E_f^* - E_{sub}^*}{E_f^* + E_{sub}^*}, \beta = \frac{\mu_f(1-2v_{sub}) - \mu_{sub}(1-2v_f)}{2\mu_f(1-v_{sub}) + 2\mu_{sub}(1-v_f)} \quad \text{Eq. 3.3}$$

where $E^* = E/(1-v^2)$ is the effective elastic modulus, v is Poisson's ratio, and μ is the shear modulus of the material. Since the total work release per unit crack propagations is the quantity of ΔE given in Eq. 3.1,

$$G_{ss} = \Delta E/h \quad \text{Eq. 3.4}$$

When small flaws are present, cracks will not begin to propagate until the residue stresses of the film exceed the steady-state requirement ($G_{ss} > \Delta E/h$) of Eq. 3.4. The function $g(\alpha, \beta)$ is computed in Figure 3.1 for most practical material combinations [53] where the value of β is between $\beta = 0$ and $\beta = \alpha/4$. The value of the function $g(\alpha, \beta)$ is low and asymptotic when the substrate is stiffer than the film ($\alpha < 0$) but grows exponentially as the substrate gets softer, resulting a larger energy release rate G_{ss} for the same residual stress σ, more prone to cracking. Qualitatively speaking, stiff films coated on soft substrates tend to crack because the softness of the substrate allows the flaws on the film to crack and propagate in the presence of residue stresses.

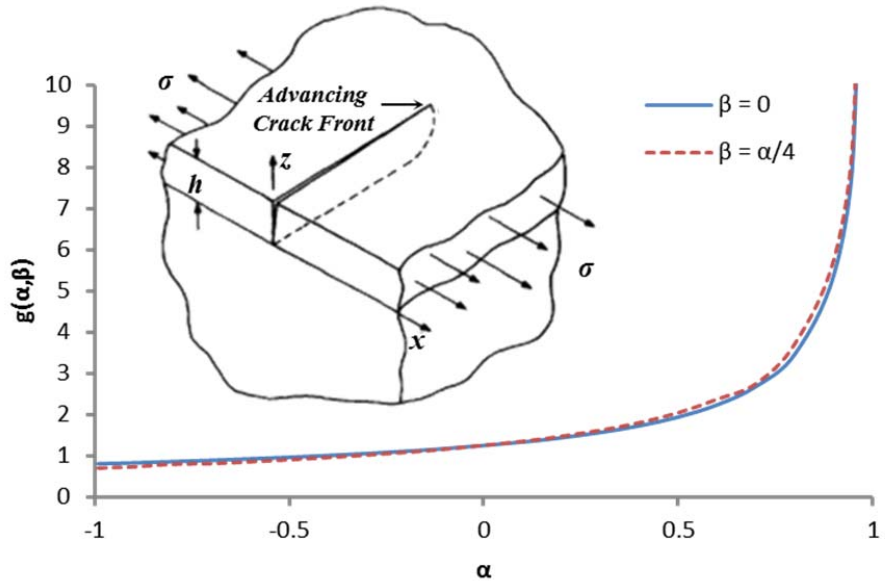

Figure 3.1: Value of function *g(α,β)* with respect to parameter *α* and *β* for the steady-state channeling of cracks in a thin film [52].

In the study, two types of experimental studies were conducted to investigate the cause of residue stresses in polydopamine thin films and the mechanical behaviour of the polydopamine thin films due to contact deformation. The results provide practical guidance on the applications of polydopamine.

3.2 Materials and Experimental

Dopamine hydrochloride was supplied by Sigma-Aldrich. TRIS-HCl buffer base (BP152) was supplied by Fisher BioReagents. Polydimethylsiloxane (PDMS, Sylgard 170) was supplied by Dow Corning Corp., Midland, MI in two components. The opaque fillers in each component were removed by centrifugation and only the remaining clear PDMS solutions were used. Plain microscope slides were supplied by Fisher Scientific and were cleaned with acetone and ultrapure water before use.

3.2.1 Preparation of Flat Sheets and Hemispherical Tips of PDMS

PDMS solution used for making elastomers was prepared by mixing the two elastomer components at a weight ratio of 10:1. The flat sheet of PDMS was made by casting 2 ml of PDMS solution onto a microscope slide and curing at 90 °C for 2.5 hours in ambient air. The sheet thickness was measured to be 1.25 ± 0.1 mm. The hemispherical tip of PDMS was made by first molding the PDMS solution into a hemispherical shape using a custom-made Teflon mold and then coating the resulting PDMS tip with a layer of PDMS solution to make the tip surface smooth. The tip core was cured at 90 °C for 15 min and the tip coating along with the core was then cured at 90 °C for 2.5 hours. The resulting tip radius was measured to be 3.0 ± 0.1 mm by analyzing the side-view image of the tip using a custom-written MATLAB (R2008a, MathWorks) script which gives a least squares best-fit to the curvature of the apex of the tip. The mechanical properties of PDMS may change overtime due to crosslinking at the room temperature. To avoid any mechanical changes before and after the coating, PDMS samples were stored in a dust-free environment at the room temperature for one month before use.

3.2.2 Coating of Polydopamine Thin Films

The dopamine solution used for coating was made by dissolving dopamine hydrochloride at a concentration of 2 mg/ml in a 10 mM TRIS-HCl buffer at pH 8.5. PDMS samples were submerged in the dopamine solution immediately for a period of 24 hours once the solution was made. To avoid the deposition of polydopamine nanoparticles formed in the solution during the coating process, all samples were placed upside down in the solution. The coated samples were rinsed with ultrapure water and dried in air overnight. The surface quality of the coatings was examined by optical

microscope (Omano OMM300T) and the thickness of the coating was measured to be 100 nm by nano-map.

3.2.3 Observation on the Formation of Cracks

Coated PDMS substrates before drying were rinsed with ultrapure water and were immediately placed under the optical microscope where the lens was focused on the surface of the substrate. Microscopic views of the surface were recorded until the coating of the substrate was fully dried in air.

3.2.4 Contact Deformation of Polydopamine Thin Films

Contact deformation measurements were carried out using a custom-made micro-indentation system that is comprised of a linear stage (Newport MFA-CC), a 25 g force transducer (Transducer Techniques GS0-25), and an inverted optical microscope (Omano OMM300T) and controlled by a custom-developed LabVIEW (version 8.5, National Instruments) program. Hemispherical PDMS tips were brought into contact with substrates of PDMS in steps of 0.5 mN until a preload force of 5 mN was detected. The tips were moved at a speed of 0.1 μm/sec between each steps with a holding time of 180 sec. The contact areas were observed to be static at the end of each step. Three sets of tests, uncoated PDMS tip on PDMS substrate (PDMS-PDMS), PDMS tip on polydopamine-coated PDMS substrate (PDMS-PDMS(D)), and polydopamine-coated PDMS tip on polydopamine-coated PDMS substrate (PDMS(D)-PDMS(D)), were conducted at the room temperature under dry conditions. Force, displacement, images of the contact area, and time information were recorded.

3.3 Results and Discussion

3.3.1 Cracking of Polydopamine Thin Films

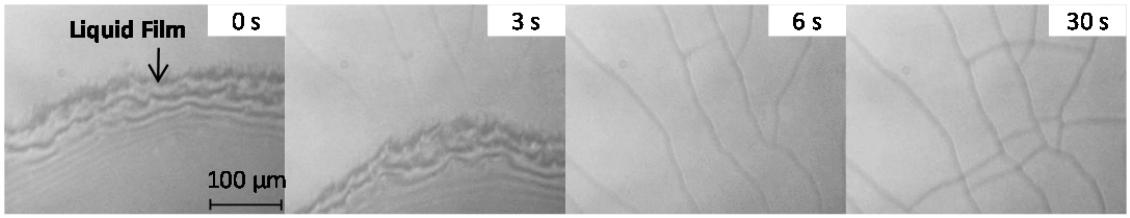

Figure 3.2: Polydopamine thin film developed micro cracks upon drying in air. The coating was prepared by immersing PDMS substrate in a 2 mg/mL fresh dopamine solution buffered by 10 mM TRIS-HCl at pH 8.5 for a period of 24 hours and was rinsed with ultrapure water before dying in air.

The physical appearance of the polydopamine thin films coated on flat PDMS substrates was carefully examined under a microscope as shown in Figure 3.2. Cracks appeared immediately after the retreat of the liquid film lingered on the coating surface. The propagation of the crack was so quick that it was impossible to observe the process and as a result, the formation of the crack appears to be instantaneous. The result indicates that the residual stresses of the film are originated from the drying process due to the contraction of the film.

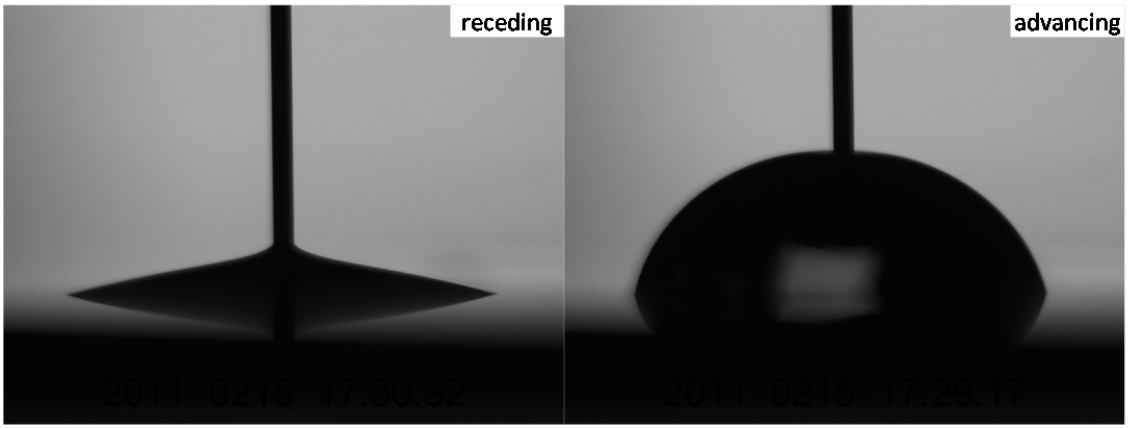

Figure 3.3: The receding and advancing water contact angles on dried polydopamine thin films. The coating was prepared by immersing PDMS substrate in a 2 mg/mL fresh dopamine solution buffered by 10 mM TRIS-HCl at pH 8.5 for a period of 24 hours and was rinsed with ultrapure water before dying in air.

As revealed in Chapter 2, polydopamine surfaces displayed a significant water contact angle hysteresis shown in Figure 3.3. Receding contact angles usually reflect liquid retention/absorption at polymers surfaces [54]. Considering that drying induces residual stresses, polydopamine thin film is likely a thin layer of gel in water which shrinks upon drying and can absorb water on its surface, explaining the low receding contact angle.

The mechanical behaviour of polydopamine thin films was studied by micro-indentation in air. The deformation behaviour of polydopamine thin films due to indentation were examined in detail and the associated images of the contact areas were shown in Figure 3.4. For PDMS(D) on PDMS(D), the contact area displayed a complete lack of contact between the two indenting polydopamine surfaces. New cracks were generated during indentation suggesting polydopamine thin films are rigid. On the other hand, for PDMS on PDMS(D), the contact area showed that the film was fully bonded and compliant to the deformation of the substrate as the edge of the contact area remained perfectly

circular during indentation process. The test can be repeated many times on the same spot without leaving any noticeable impacts on the integrity of the film (no new cracks) and on the force-displacement data collected. This suggests polydopamine thin films were strongly bonded to the underlying substrate and were fairly robust. Due to poor contact, no useful data could be extracted from PDMS(D) on PDMS(D) while the data from PDMS on PDMS and from PDMS on PDMS(D) were analyzed in the framework of JKR contact mechanics in the next subsection.

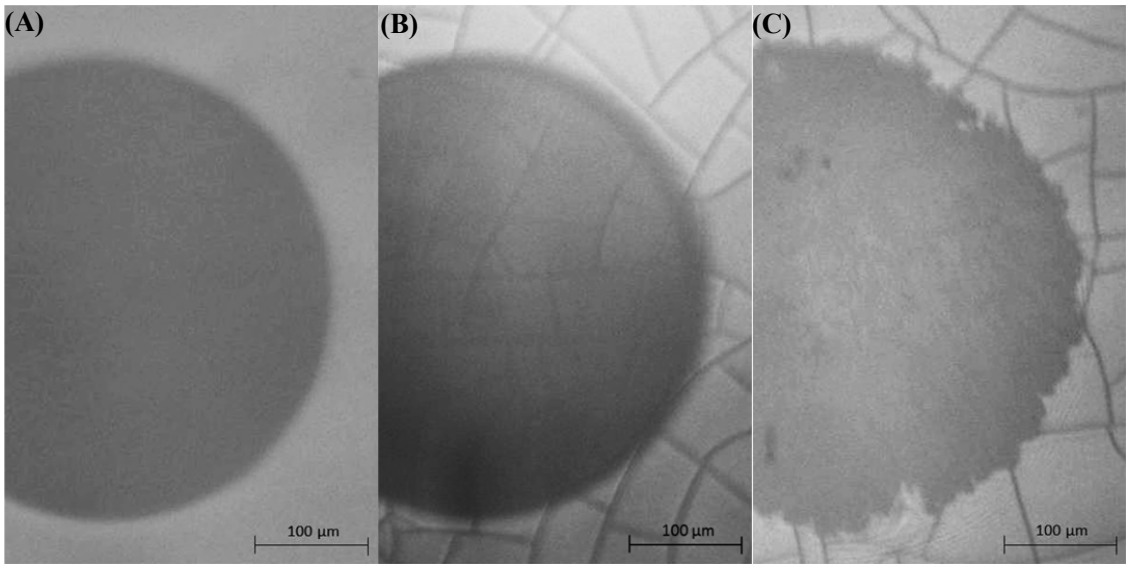

Figure 3.4: Contact deformations of (A) PDMS on PDMS, (B) PDMS on PDMS(D), and (C) PDMS(D) on PDMS(D) during micro-indentation processes.

We have attempted to repeat this experiment for wet conditions but could not do so because the contact areas were invisible in water. In the study of the role of melanin in mechanical properties of Glycera jaws, the mechanical properties of the *Sepia* melanin particles and the constituent melanin of the jaw were probed through nano-indentation [55]. It was reported that when hydrated, the elasticity of the *Sepia* melanin dropped by a factor of about 4, of which, the precipitous drop was likely associated with absorption of water into the aggregates via the pore spaces between adjoining granules. Such pathways for water access are absent in the *Sepia* melanin granules themselves and the melanin structure produced by jaw hydrolysis. In contrast, the elasticity of the constituent melanin only dropped in the range of 15-25% due to hydration. As polydopamine are structured much similar to the constituent melanin [56], the mechanical behaviours of polydopamine measured here in dry conditions should also reflect its behaviours in wet conditions, but this correlation should be regarded with cautions.

3.3.2 Mechanical Analysis based on JKR Contact Mechanics

Figure 3.5 plots the typical cubic contact radius vs. force curves for micro-indentations with and without the bonded film. JKR fits well with the data of the coated substrate, suggesting the coated substrate acts as a homogeneous half-space. The curves were analyzed in the framework of JKR contact mechanics revealing a work of adhesion of 38.9 and 41.5 $\mathrm{mJ/m^2}$ and a combined (tip and substrate) effective elastic modulus of 0.49 and 0.48 MPa, with and without the film, respectively. The work of adhesion of pure PDMS is well within the range of 40 $\mathrm{mJ/m^2}$ to 44 $\mathrm{mJ/m^2}$ reported in literatures [57-60] and the work of adhesion for polydopamine coated PDMS is lower than the value predicted by theoretical calculations.

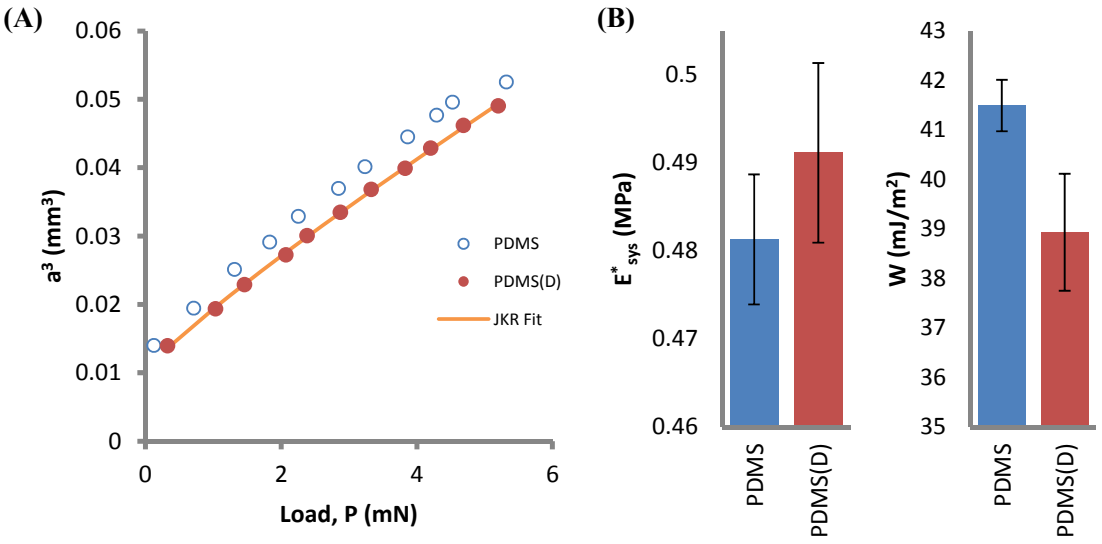

Figure 3.5: Typical cubic contact radius (a^3) and Load (P) curves (A) of micro-indentation of hemispherical PDMS tips on flat PDMS substrates coated with and without polydopamine thin films (PDMS and PDMS(D)) and the associated effective elastic modulus (E^*_{sys}) and work of adhesion (W) with one standard deviation (B) determined by the JKR theory.

The surface free energy of polydopamine was determined by contact angle measurements using van Oss's method. Detailed results are present in Chapter 5. The dispersive and polar surface energy components of polydopamine were determined to be 30 $\mathrm{mJ/m^2}$ and 10 $\mathrm{mJ/m^2}$, respectively. Assuming a geometric combination rule (van Oss) and the surface energy components of 20.8 $\mathrm{mJ/m^2}$ and 0 $\mathrm{mJ/m^2}$ for pure PDMS, the work of adhesion between polydopamine and PDMS is estimated to be $2\sqrt{20.8 \times 30} = 50.0\ \mathrm{mJ/m^2}$, which is higher than the value, 38.9 $\mathrm{mJ/m^2}$, determined by

contact mechanics. This discrepancy can be explained by the fact that the film is fairly stiff that its contact with the PDMS surface is likely imperfect leading to a lower theoretical work of adhesion.

The large deviation of the effective elastic modulus is mainly caused by sample to sample variations. Comparing the same sample and the same contact spot with and without the film revealed a difference of 0.1 MPa with a standard deviation of less than 30 kPa, that is, the elasticity measured was always higher with coating. This consistency is suprising and it has motivated us to estimate the elasticity of the thin film based on this elastic difference. Subsequently, we extended the JKR theory by accommodating the mechanics of thin films, for which we name this new theory "thin film contact mechanics". The detailed derivations and experimental validations of the theory are present in Chapter 4, with discussions of the technical implications of the technique and comprehensive reviews of JKR contact mechanics.

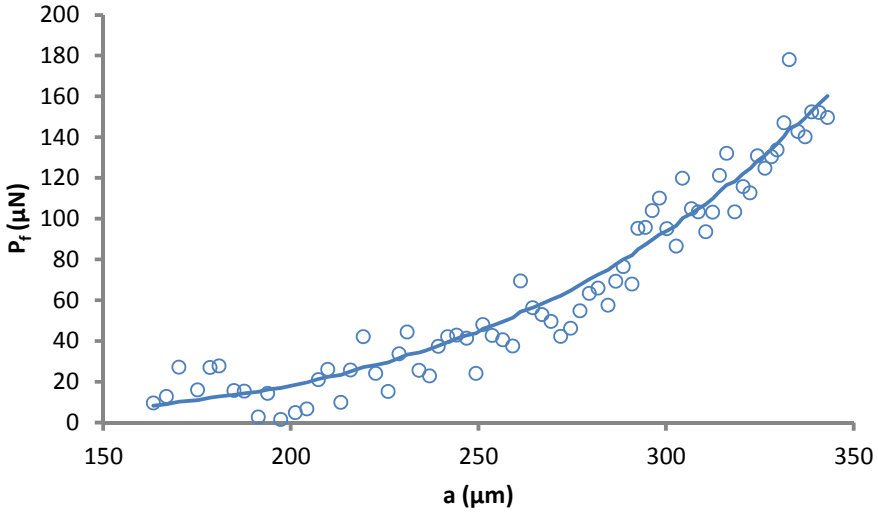

Figure 3.6: Typical plot of the applied load (P_f) of the thin film against the contact radius (a). Data are generated based on the difference in the elasticity of the substrate with and without the film (round empty dot) and are fitted based on the plate theory (line) with the substitution of experimental data.

From the combined effective elastic modulus, the effective elastic modulus for the substrate with and without the film are 0.96 and 1.0 MPa, respectively. Based on thin film contact mechanics, the effective elastic modulus of polydopamine thin films was determined to be 7 GPa by correlating the load caused by the elastic difference with the load due to the film deformation as shown in Figure 3.6. Even though the effect of cracks on the deformation of the film is not very significant, as discussed in

Chapter 4, it still affects the result so that the actual elasticity of the film should be a bit higher. This determined elasticity is reasonable as it falls in the 3 GPa to 7 GPa range of melanin [55].

3.4 Conclusions

Two types of experimental studies had been performed to investigate the mechanical behaviour of polydopamine thin films coated on PDMS substrates. Observations from the drying process suggest the polydopamine thin film is a layer of gel which shrinks if dehydrated. Extra attentions should be paid if polydopamine thin film is used as a composite material, i.e. as a sub-layer of a membrane, as the shrinkage of the film can introduce undesired residual stresses to the system. The contact deformation study showed that the polydopamine thin film is strongly bonded to the substrate and is fairly robust as it complied fully with the deformation of the substrate during indentation and stood intact after repeat indentations. Analyzing the contact deformation in the framework of JKR and thin film contact mechanics revealed an effective elastic modulus of 7 GPa for polydopamine. Therefore, it is recommended to coat/joint polydopamine with substrates stiffer than 7 GPa as anything softer would make polydopamine prone to cracking, undermining its integrity. In general, it is not recommended to dry polydopamine for any applications unless drying is absolutely necessary.

Chapter 4
Thin Film Contact Mechanics

4.1 Introduction

The subject of contact mechanics has started in 1882 with the publication by Heinrich Hertz of his classic paper, "On the contact of elastic solids" [61]. Hertz's theory modeled the contact deformation between two elastic bodies with curved smooth and non-adhering surfaces, providing the foundation for modern contact mechanic theories. The theory has been extended to account for the contact of rough elastic and viscoelastic materials [62-64]. The most important advancement in the field of contact mechanics in the mid-twentieth century may be attributed to Johnson, Kendall, and Roberts (JKR) for which their extended theory accounts for adhesive contacts by balancing the elastic energy associated with the deformation of the bodies, the potential energy associated with the displacement of the bodies, and the work of adhesion associated with the contact of the bodies [65]. Although the JKR theory only models ideally smooth and elastic spheres interacting through equilibrium adhesive forces, covering only a relatively narrow subset of adhesive contact problems, it had an enormous and ongoing impact on both the scientific and engineering communities, attributing to the fact that adhesive forces become more important as the contacting bodies reduce in stiffness and size [66]. It has been used extensively in surface and adhesion science for various applications including the direct measurements of surface and interfacial energies of polymers [67] and monolayers [68], quantitative studies on the role of interfacial coupling agents in the adhesion of elastomers [69], and the adhesion of micro-particles on surfaces [70].

There is a continuing interest in the application of contact mechanics to thin elastic coatings, films and multilayers, i.e. pressure-sensitive adhesives, anti-wear coating, microelectronics, optical systems, and micro electro mechanical systems (MEMS). As a result, numerous models of layered systems were established in the framework of JKR contact mechanics including an elementary theory for a rigid spherical indenter contacting a thin elastic coating bonded to a rigid substrate [71], a numerical model of the adhesion between a spherical indenter and a stiff elastic substrate with a compliant elastic coating [72, 73], and a finite element analysis of layered elastic materials between a rigid indenter and a rigid substrate [74, 75]. In this study, we have extended the JKR theory to accommodate the mechanics of a stiff elastic thin film bonded to a flat elastic substrate. We denote this new theory "thin film contact mechanics". It is important to note that the mechanics of this theory

is fundamentally different from the ones mentioned above. In the previous works, soft thin films are bonded to stiff substrate and the mechanical property of the film is determined by compression or in other words, is determined from the film's shortest dimensions. The physical situation is the opposite in our system for which the thin films are stiffer than the substrate. Upon indentation, the film is stretched and bended instead of being compressed because the substrate is softer. Accordingly, the mechanical property of the film in our theory is determined from its longest dimensions making the approach more accurate and reliable.

The thin film contact mechanics can provide accurate and reliable quantitative measurements of the effective elastic modulus of nanometer thin layers and can probably be used to investigate the interfacial behaviours between the layers. We believe it is valuable for nanotechnology research because: (i) nano-fabrications are based on deposition of material layers patterned by self-assembly and nanolithography [76]; (ii) the mechanical behaviour of nanometer thin layers is thickness dependent due to the influences of surface atoms [77-80]. The binding situation (free energy) of atoms near a surface is different than atoms in the bulk because of the corresponding redistribution of electronic charge due to reduced coordination [81]; and (iii) the effective elastic modulus is one of the most important parameters defining the compatibility of bonded layers where mismatching of elastic modulus of the layers can lead to delamination and buckling of the composite material [82]. Additionally, the technique might be naturally suitable for soft-substrate based applications such as wearable electronics [76].

Nano-indentation is one of the most prevailing techniques for measuring nanometer thin film properties, of which, a hard pointed probe is pressed into a thin film and the properties of the film is determined by the elastic retraction of the indent upon unloading of the probe [83]. In comparison, thin film contact mechanics offers the following advantages: (i) more realistic deformation of the thin film, i.e. bending and stretching vs. hole-punching; (ii) better measurement dependability, i.e. contact area vs. point measurements. In nano-indentation, the data measured from point to point tends to vary and scatter, especially if the quality of film is not consistent (i.e. rough surfaces); (iii) sounder theoretical basis. The thin film contact mechanics accounts for both the adhesive contact and the substrate's mechanical properties by definition while nano-indentation does not. Consequently, the nano-indentation measurement of the elastic modulus of thin films is affected by the substrates as the elastic field under the indenter is not confined to the film itself but extending to the substrate. The influence can be observed even at an indentation depth of less than 10% of the film thickness for a

500 nm thin Al layer deposited on Si [84]. In these cases, the modulus is commonly estimated with the relatively simple King's numerical analysis [85] but the analysis becomes significantly inaccurate when the film gets thinner (i.e. < 200 nm) since one must assume a flat geometry for non-flat probes [84] and becomes inapplicable when the film is stiffer than the substrate as one must assume the film hardness is constant with respect to the indentation depth until the indenter is close to the film–substrate interface [86]. Formal treatments involving numerical solution of complex exact analytical functions [87] or finite element calculations [88] must be used to determine the elasticity accurately [89]. The data analysis of nano-indentation is almost always based on non-adhering contact, which is usually reasonable as the contacts are normally hard-on-hard. However, it has been shown with a spherical diamond probe that if adhesive forces were present, the data analysis should be carried out according to JKR's model rather than Hertz or else the elastic modulus calculated would be way-off [90]. It is unclear on how to interpret the nano-indentation data if one has to account for both the substrate effect and the adhesion effect; and (iv) less sensitivity to environmental factors. This means less instrument related errors and fewer limitations on how the experiment can be conducted, i.e. micro-indentations can be performed underwater.

The disadvantage of the thin film contact mechanics is that the precision of its result is highly dependent on the precision of the instrument. In the subsequent sections, we will first review the key equations and assumptions of JKR contact mechanics, then we will provide a detailed derivation on the thin film contact mechanics, and finally, we will validate our theory against gold thin films of nanometer thickness.

4.2 Review of JKR Contact Mechanics

Derivations of JKR contact mechanics can be found in [91] and are not covered in this section.

JKR contact mechanics states the following relations for two spherical elastic bodies (tip and substrate) in contact:

$$P_{sys} = P_{sys}^{e} - P_{sys}^{a} = \frac{4E_{sys}^{*}a^{3}}{3R_{sys}} - \sqrt{8\pi a^{3}W_{sys}E_{sys}^{*}} \qquad \text{Eq. 4.1}$$

$$E_{sys}^{*} = \left(\frac{1}{E_{tip}^{*}} + \frac{1}{E_{sub}^{*}}\right)^{-1}$$

$$R_{sys} = \left(\frac{1}{R_{tip}} + \frac{1}{R_{sub}}\right)^{-1}$$

P_{sys} is the applied load of the system, which can be split into two independent components, an elastic component, P_{sys}^{e}, and an adhesive component, P_{sys}^{a}. a is the contact radius, which is the radial distance from the center of contact to the edge of the area in contact. W_{sys} is the thermodynamic work of adhesion between the surfaces of the two elastic bodies. R_{sys} is the combined radius of the tip and the substrate and E_{sys}^{*} is the combined effective elastic modulus. If the substrate is flat, the combined radius becomes the radius of the tip. The effective elastic modulus (E^{*}) is related to the Young's modulus (E) and the Possion's ratio (v) by

$$E^{*} = \frac{E}{1 - v^{2}} \qquad \text{Eq. 4.2}$$

JKR contact mechanics employs the following assumptions:

1. The system is in mechanical equilibrium.
2. The contact deformation is small compared to the size of the bodies, so:
    a. The bodies can be considered as a mathematical half-space.
    b. Parabolic approximation can be assumed for the profile of spheres as the contact radius is much smaller than the radius of the bodies.
    c. The radial displacement (u) due to deformation is much smaller than the normal displacement (w).
3. Elastic and adhesive forces are confined within the contact area, meaning:
    a. The normal stress is zero outside of the contact area.
    b. The molecular interfacial forces are infinitesimally short ranged.

    The implication for adhesion is controversial. An alternate theory, developed by Derjaguin, Muller, and Toporov (DMT), assumes the molecular forces have a finite range and only act outside the contact area. Both theories are valid for certain physical situations. In general, it is agreed that the DMT theory would be appropriate for a hard solid of low surface energy and small radius of curvature and the JKR theory would be more accurate for soft materials with relatively high surface energy and large radius of curvature. Quantitatively speaking, JKR is valid when the Tabor's dimensionless parameter (μ) [92] is greater than 5, where

$$\mu = \left(\frac{RW^2}{\frac{16}{9} E^{*2} z_o^3} \right)^{1/3} \quad \text{Eq. 4.3}$$

z_o is the equilibrium separation distance of the atoms on the surfaces of the contacting bodies and is approximately 0.3 nm for apolar surfaces.

4. The surfaces of the bodies are frictionless, so:
    a. The contacting surfaces can slide against each other.
    b. Only normal stress is transmitted between bodies against the load.

    Although it normally makes little to no practical differences, the assumption is generally not appropriate for rough or adhering materials. One way to void the assumption is to have the identical elastic properties (same E and v) for both bodies so their surfaces would slide together. Under this condition, small-scale roughness will only affect adhesion but not elasticity of the system. It has been shown that in practice [92], roughness only affects mostly adhesion and the effect is negligible if the contact is soft and the mean asperity height of the roughness is less than 100 nm.

4.3 Derivation of Thin Film Contact Mechanics

Thin film contact mechanics models the contact between a spherical elastic tip and a flat elastic substrate bonded with a thin layer of elastic film, in which the film is harder than the substrate.

We assume the coated substrate will act as a homogeneous half-space, meaning the bulk effective elastic modulus of the coated substrate is constant during indentation. The assumption is generally valid because the film is very thin. It has been shown that the coated substrate behaves homogeneously when a thin polymer film is directly coated onto a substrate with a low elastic modulus ($E < 10$ MPa) and when the ratio of contact radius to film thickness is large ($a/h > 20$) [93].

The subscript, "(f)" indicates "with thin film". For a system with bonded film, Eq. 4.1 becomes

$$P_{sys(f)} = P^e_{sys(f)} - P^a_{sys(f)} = \frac{4E^*_{sys(f)} a^3}{3R_{sys}} - \sqrt{8\pi a^3 W_{sys(f)} E^*_{sys(f)}} \quad \text{Eq. 4.4}$$

$$E^*_{sys(f)} = \left(\frac{1}{E^*_{sub(f)}} + \frac{1}{E^*_{tip}}\right)^{-1}$$

$$R_{sys} = \left(\frac{1}{R_{sub}} + \frac{1}{R_{tip}}\right)^{-1}$$

When the film is harder than the substrate, the deformation of the substrate is constrained by the film such that a higher applied load is required to reach the same contact radius. We attribute the difference in load to the deformation of the film. With respect to elastic and adhesive components of the system, the difference is

$$\boxed{P_f = P_{sys(f)} - \frac{4E^*_{sys}a^3}{3R_{sys}} + \sqrt{8\pi a^3 W_{sys(f)} E^*_{sys}}} \qquad \text{Eq. 4.5}$$

The plate theory is applied to model the deformation of the film as the film fits the definition of a plate, which is a flat non-curved solid whose thickness is at least an order of magnitude smaller than the smallest of its other dimensions [94]. A plate deforms by bending and by stretching when its normal deflection or displacement is larger than one fifth of its thickness. Based on the geometric symmetry of the system and the first assumption of JKR, the deformation can be approximated by mechanical equilibrium using a simplified form of von Kármán's equations [94]

$$\boxed{\frac{\mathrm{d}^3 w}{\mathrm{d}r^3} + \frac{1}{r}\frac{\mathrm{d}^2 w}{\mathrm{d}r^2} - \frac{1}{\mathrm{r}^2}\frac{\mathrm{d}w}{\mathrm{d}r} = \frac{12}{h^2}\frac{\mathrm{d}w}{\mathrm{d}r}\left[\frac{\mathrm{d}u}{\mathrm{d}r} + v_f\frac{u}{r} + \frac{1}{2}\left(\frac{\mathrm{d}w}{\mathrm{d}r}\right)^2\right] + \frac{12}{h^3 E^*_f r}\int_0^r p_z(r) r \mathrm{d}r} \qquad \text{Eq. 4.6}$$

w is the normal displacement of the film under the applied normal stress, $p_z(r)$, u is the radial displacement of the film, and r is the radial distance from the center of contact. v_f, E^*_f, and h are the Possion's ratio, the effective elastic modulus, and the thickness of the film. With respect to the second assumption of JKR

$$u \ll w \rightarrow \begin{cases} u = 0 \\ \mathrm{d}u/\mathrm{d}r = 0 \end{cases} \qquad \text{Eq. 4.7}$$

Eq. 4.6 becomes

$$\frac{\mathrm{d}^3w}{\mathrm{d}r^3}+\frac{1}{r}\frac{\mathrm{d}^2w}{\mathrm{d}r^2}-\frac{1}{\mathrm{r}^2}\frac{\mathrm{d}w}{\mathrm{d}r}=\frac{6}{h^2}\left(\frac{\mathrm{d}w}{\mathrm{d}r}\right)^3+\frac{12}{h^3E_f^*r}\int_0^r p_z(r)r\mathrm{d}r \qquad \text{Eq. 4.8}$$

In JKR contact mechanics, the curvature of the deformation within the contact area is only dependent on the elastic component of the system. Hence, the shape of deformation is spherical, just like Hertz, and has an equivalent rigid tip radius of

$$\boxed{R^+=\frac{\frac{4}{3}E_{sub(f)}^*a^3}{P_{sys(f)}+\sqrt{8\pi a^3W_{sys(f)}E_{sys(f)}^*}}} \qquad \text{Eq. 4.9}$$

Accordingly, the normal displacement of the film can be related to the radial distance as shown in Figure 4.1, where *c* is a constant

$$w=\sqrt{(R^+)^2-r^2}\ -c \text{ for } 0\le r\le a \qquad \text{Eq. 4.10}$$

Substituting the derivatives of dw/dr, Eq. 4.8 becomes

$$\int_0^r p_z(r)r\mathrm{d}r=E_f^*h\frac{-6r^6+6r^4(R^+)^2+h^2r^4-4h^2r^2(R^+)^2}{12((R^+)^2-r^2)^{5/2}} \qquad \text{Eq. 4.11}$$

As the film is compliant to the deformation of the substrate and according to the third assumption of JKR, only normal stress is transmitted within the contact area. With respect to the contact radius and Eq. 4.11, the applied load due to bending and stretching of the film is

$$\boxed{P_f=2\pi\int_0^a p_z(r)rdr=\pi E_f^*h\left(\frac{-6a^6+6a^4(R^+)^2+h^2a^4-4h^2a^2(R^+)^2}{6((R^+)^2-a^2)^{5/2}}\right)} \qquad \text{Eq. 4.12}$$

When the film is equal to or softer than the substrate ($E_f^*\le E_{sub}^*$), the applied load calculated from Eq. 4.12 is very small but not zero. The load is both physically unrealistic and inconsistent with Eq. 4.5. The discrepancy is due to the fact that the deformation of the film is dominated by compression when the substrate is harder than the film, which makes the film thickness a variable during indentation, violating the basic premise of the plate theory.

In practice, the effective elastic modulus of a thin film can be obtained by comparing a system with and without bonded film using Eq. 4.5 and fitting the difference with Eq. 4.12. The method will be demonstrated in the next section. We recommend the following experimental practices to improve the techniques' accuracy: (i) use tips and substrates of the same mechanical properties. This gets around the forth assumption of JKR and minimizes the influence of surface imperfections such as small-scale roughness on the measuring of system elasticity; and (ii) use soft tips and substrates. This avoids the discrepancy mentioned above and also prevents the destruction of the film during indentation.

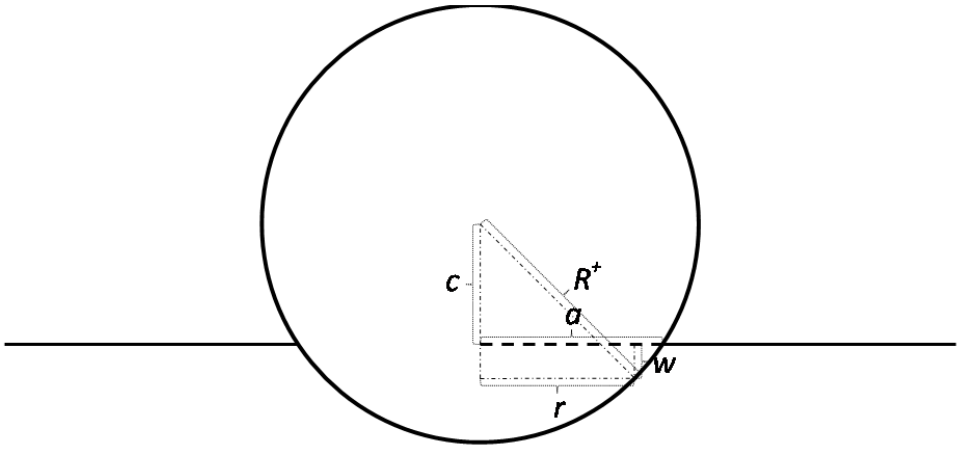

Figure 4.1: Geometric relationship between the radial distance, *r*, equivalent radius, R^+, and the normal displacement, *w*, where *c* is a constant.

4.4 Materials and Experimental

Polydimethylsiloxane (PDMS, Sylgard 170) was supplied by Dow Corning Corp., Midland, MI in two components. The opaque fillers in each component were removed by centrifugation and only the remaining clear PDMS solutions were used. Plain microscope slides were supplied by Fisher Scientific and were cleaned with acetone and ultrapure water before use.

4.4.1 Preparation of Flat Sheets and Hemispherical Tips of PDMS

PDMS solution used for making elastomers was prepared by mixing the two elastomer components at a weight ratio of 10:1. The flat sheet of PDMS was made by casting 2 ml of PDMS solution onto a microscope slide and curing at 90 °C for 2.5 hours in ambient air. The sheet thickness was measured to be 1.25 ± 0.1 mm. The hemispherical tip of PDMS was made by first molding the PDMS solution

into a hemispherical shape using a custom-made Teflon mold and then coating the resulting PDMS tip with a layer of PDMS solution to make the tip surface smooth. The tip core was cured at 90 °C for 15 min and the tip coating along with the core was then cured at 90 °C for 2.5 hours. The resulting tip radius was measured to be 3.0 ± 0.1 mm by analyzing the side-view image of the tip using a custom-written MATLAB (R2008a, MathWorks) script which gives a least squares best-fit to the curvature of the apex of the tip. The mechanical properties of PDMS may change overtime due to crosslinking at the room temperature. To avoid any mechanical changes before and after the coating, PDMS samples were stored in a dust-free environment at the room temperature over three months before use.

4.4.2 Deposition of Gold Thin Films

Gold thin films were deposited on flat sheets of PDMS in a magnetron sputter-coater (Denton Vacuum Desk II) at 15 mA under room temperature. The thickness of the deposited film was controlled by deposition time (50 nm for 600 sec) and was measured by AFM. According to AFM, the topology of the film contained no noticeable crystallographic texture indicating the film is polycrystalline.

4.4.3 Contact Deformation of Gold Thin Films

Contact deformation measurements were carried out using a custom-made micro-indentation system that is comprised of a linear stage (Newport MFA-CC), a 25 g force transducer (Transducer Techniques GS0-25), and an inverted optical microscope (Omano OMM300T) and controlled by a custom-developed LabVIEW (version 8.5, National Instruments) program. Hemispherical PDMS tips were brought into contact with substrates of PDMS at a speed of $0.1\ \mu m/sec$ until a certain preload force was reached. Then, the substrates were coated with gold and the indentation was repeated with the same tips on the same contact spots. Force, displacement, images of the contact area, and time information were recorded. Static indentations were also conducted with the tip moving at $0.1\ \mu m/sec$ between steps and holding for 180 sec at each step on gold coated samples to check if the indentation meets the first assumption of JKR contact mechanics. Essentially, no substantial changes in contact areas or forces were detected during each step of loading. This suggests the loading speed, $0.1\ \mu m/sec$, was quasi-equilibrium.

4.5 Results and Discussion

4.5.1 Effect of Plastic Deformation

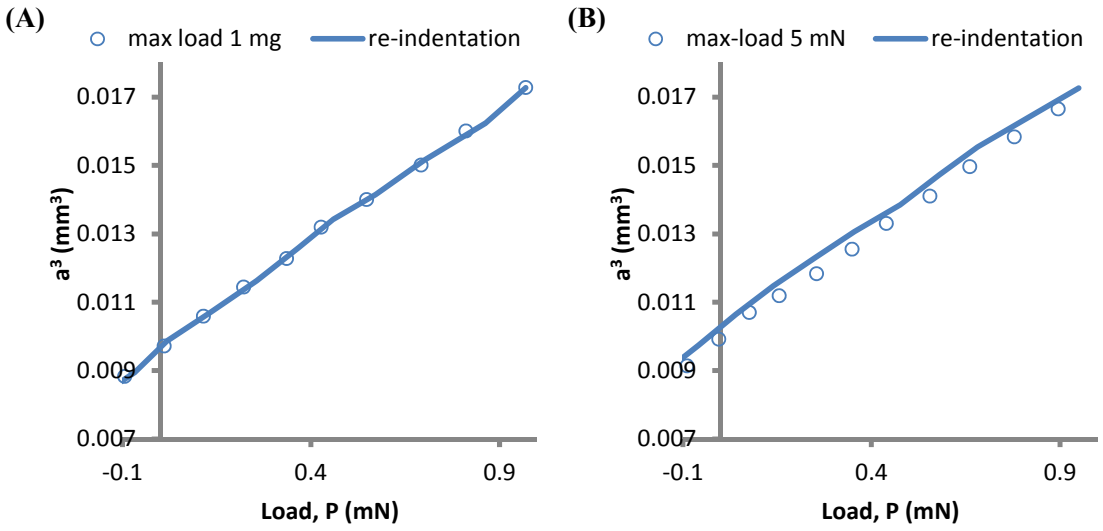

Figure 4.2: Typical cubic contact radius (a^3) and load (P) curves of micro-indentation and re-indentation of hemispherical PDMS tips on flat PDMS substrates coated with 50 nm gold thin films at 1 mg preload (A) and at 5 mg preload (B).

Gold is one of the most ductile metals of all. While it has a bulk Young's modulus of 79 GPa, its tensile strength is only around 120 MPa. As a result, plastic deformation of gold thin films due to indentation is expected. To identify the transition of deformation from elastic to plastic, micro-indentation and re-indentation of gold coated PDMS substrates were performed at different preloads. Figure 4.2 shows the typical cubic contact radius and load curves at 1 mg and 5 mg preloads with re-indentation. The contact deformation from re-indentation was identical to that of the initial indentation for 1 mg preload. In contrast, for a preload of 5 mg, the deformation was greater, that is, the contact area is larger for the same applied load, suggesting the gold thin film was permanently distorted by the initial indentation. The repeatability of the indentation process suggests that the deformation is mostly elastic for indenting at 1 mg preload and plastic deformations do occur and are significant at higher preloads. We suspect the plastic deformation is likely a result from the unloading process rather than from loading process because the pull-off forces from unloading is higher than the preload from loading, the loading data fit well with JKR contact mechanics, and it was observed in some experiments that the thin films were not visibly damaged (cracking) until the unloading process.

4.5.2 Effect of Cracks

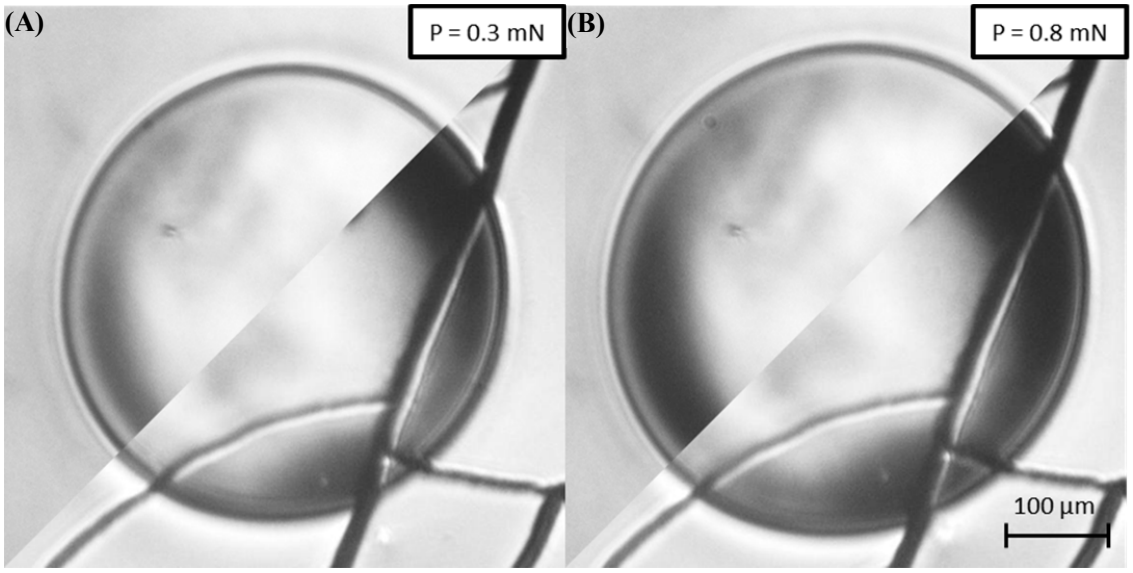

Figure 4.3: Comparison of typical contact deformations of 100 nm gold coated PDMS substrate with (bottom right corner) and without cracks (top left corner) on the same contact spot using the same tip at an applied load of 0.3 mN (A) and 0.8 mN (B) during micro-indentation.

As discussed previously in Chapter 3, it is hard to avoid the formation of cracks on thin films when the films contain residue stresses and are stiffer than the substrates coated by the films. Since the thin film contact mechanics aims specifically for stiff thin films bonded to soft flat substrates, it is important to address the effect of cracks. Tests at 1 mN preload were carried out to examine the contact deformation of gold thin films with and without cracks by first indenting on a spot without cracks, then inducing cracks to the spot by stressing the film at a point distant from the contact area, and finally re-indenting on the same spot with the same tip. Figure 4.3 shows the deformation at the contact spot with and without cracks at different applied loads. As shown by the images, the size of the contact area was the same with and without cracks at a given load, suggesting that cracks have minor effects on the indentation result. This is reasonable considering that the film was fully bonded and compliant to the deformation of the substrate and the influence of cracks on the deformation of the substrate was limited as the edge of the contact area was not visibly distorted by the presence of cracks.

4.5.3 Mechanical Analysis by Thin Film Contact Mechanics

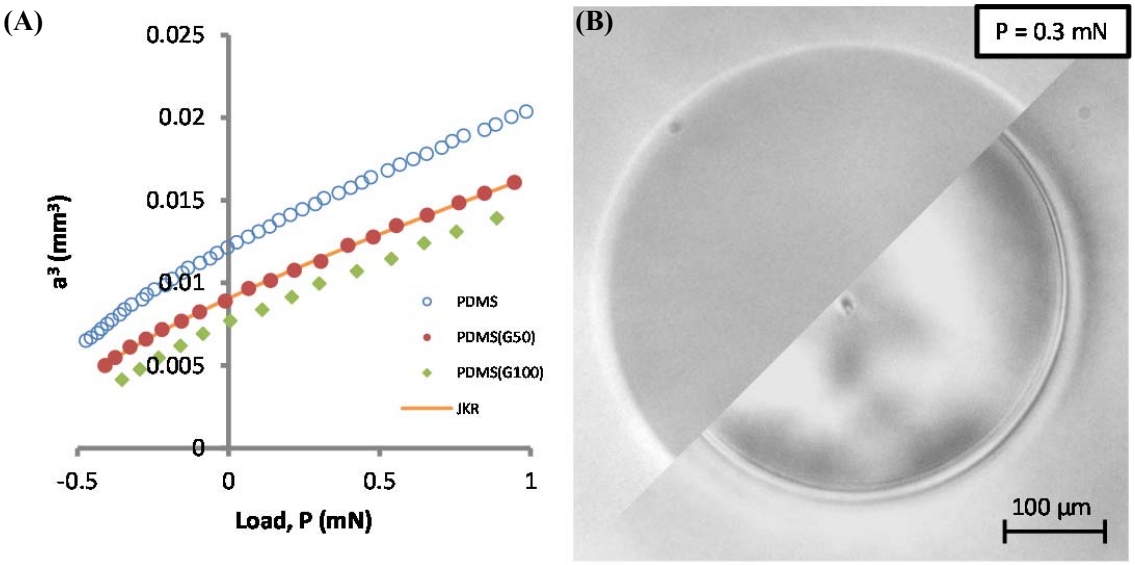

Figure 4.4: Typical cubic contact radius (a^3) and Load (P) curves (A) of micro-indentation of hemispherical PDMS tips on flat PDMS substrates (PDMS) coated with 50 nm and 100 nm thick gold thin films (PDMS(G50) and PDMS(G100)) and the associated contact deformations (B) with (bottom right corner) and without 100 nm coating (top left corner) at an applied load of 0.3 mN.

Figure 4.4A plots the typical cubic contact radius vs. force curves for micro-indentations with and without the bonded film. As shown in Figure 4.4B, the contact area of the coated substrate was significantly smaller than the one without coating at the same applied load, indicating the film had constrained the deformation of the substrate. To discount plasticity, only data within an applied load of 1 mN were analyzed in the framework of JKR contact mechanics. The data of coated samples fitted well with JKR, which confirms that the coated substrate acted as a homogeneous half-space.

For uncoated samples, the work of adhesion ranged from 43.1 to 44.7 mJ/m^2 and the combined effective elastic modulus ranged from 0.469 to 0.475 MPa. The work of adhesion of PDMS was within the range of 40 mJ/m^2 to 44 mJ/m^2 reported in literatures [59-61]. For coated samples, while the combined elastic modulus only ranged from 0.518 to 0.521 MPa and from 0.543 to 0.546 MPa for 50 nm and 100 nm thickness, the work of adhesion between gold and PDMS varied significantly, ranging from 32.2 to 43.7 mJ/m^2. Surface contaminations and rigidity of the gold surface could play a role for the variation as metals are highly energetic and rigid compared to PDMS elastomers. From the combined effective elastic modulus of the system, the modulus for the substrate with the film

ranged from 1.24 to 1.26 MPa and 1.29 MPa to 1.31 MPa for 50 nm and 100 nm thicknesses and without the film ranged from 0.938 to 0.950 MPa.

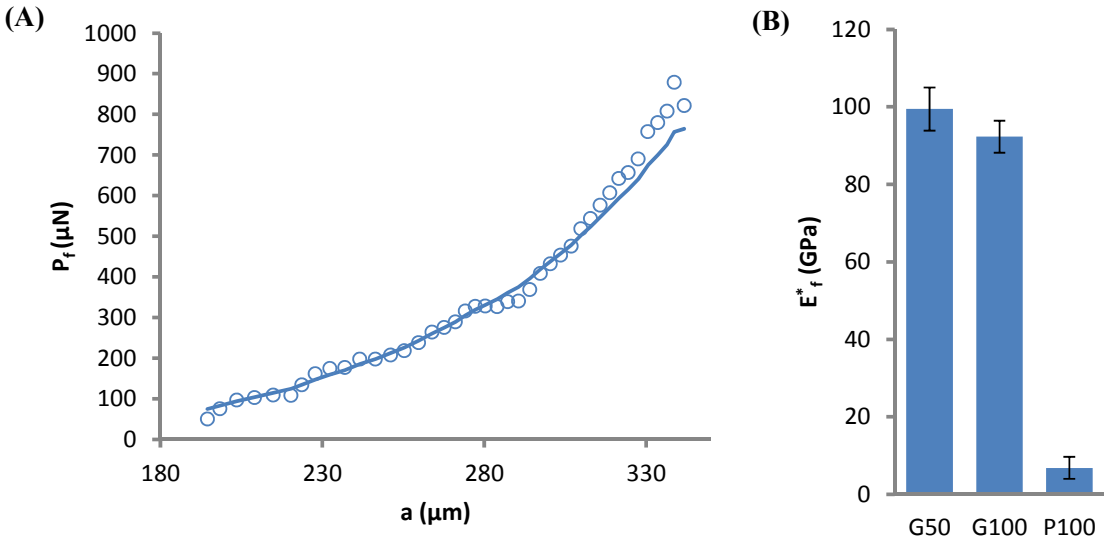

Figure 4.5: Typical plot (A) of the applied load (P_f) of the 50 nm gold thin film against the contact radius (a) and the fitted effective elastic modulus with one standard deviation for 100 nm polydopamine thin films (P100) and the gold thin film of 50 nm (G50) and 100 nm (G100) thickness (B). Data are generated based on the difference in the elasticity of the substrate with and without the film (round empty dot) and are fitted based on the plate theory (line) with the substitution of experimental data. Fitting were performed on data within the applied load of 1 mg to discount plasticity of the film.

Figure 4.5A shows the typical plot of the applied load of the film against the contact radius. The elastic behaviour of the film, shown as empty dots in the plot, was predicted by the elastic difference of the system as described by Eq. 4.5. Based on the equivalent rigid tip radius and the plate theory, Eq. 4.9 and Eq. 4.12 were employed to fit the predicted elastic behaviour. Experimental data were substituted into the equations wherever possible. Assuming the film is fully elastic before the indentation reaches an applied load of 1 mN, the fitting was performed on experimental data below that load. As shown in Figure 4.5B, the effective elastic modulus of gold thin films was determined to be 99 GPa and 92 GPa for 50 nm and 100 nm thicknesses. The modulus of 100 nm thick polydopamine thin film from Chapter 3 is plotted here for comparison. The modules of gold thin films are remarkably in good agreement with the documented polycrystalline bulk gold modulus of 98 GPa (with Young's modulus of 79 GPa and Poisson's ratio of 0.44). The agreement is not

surprising as it has been demonstrated from nano-indentation experiments that the elastic behaviour of gold thin films ($40\ \text{nm} < h < 800\ \text{nm}$) are consistent with that of bulk [86, 89].

Although we have only fitted the data within a load of 1 mN, accounting for all the data, the fitted curve does not deviate much from the predicted curve generated by the elastic difference beyond the applied load. This suggests plasticity was unlikely a factor during the loading process. The result agrees with our observations on the repeatability of the indentation process. Furthermore, the engineering strain the gold thin film experienced during indentation was too small to show plastic behaviour. The engineering strain (ϵ_e) of a film at a given load can be roughly estimated using the arc of the deformation and the diameter of the contact area, where the unit of the angle from the inverse sin function is in radian

$$\epsilon_e = \frac{\Delta L}{L} = \frac{R^+ \sin^{-1}\left(\frac{a}{R^+}\right) - a}{a} \qquad \text{Eq. 4.13}$$

The estimated engineering strain of the gold thin film ranged from 0.01% to 0.05% during loading of the indentation process. Most materials obey Hooke's law to a reasonable degree that they do not deform plastically until a certain strain is reached. For bulk ductile metals such as the annealed polycrystalline copper, this strain is around 0.01% [95]. However, for thin ductile metal films, the strain tends to be much higher due to physical constraints imposed by the film dimensions on the plastic flow of atoms in the film. It has been shown that gold films were increasingly stronger than bulk gold as the film gets thinner, i.e. the stain is more than 0.2% for a film thickness of 800 nm [96, 97].

4.6 Conclusion

In conclusion, we have validated thin film contact mechanics against gold thin films of two different thicknesses, 50 nm and 100 nm. The effective elastic modulus of gold thin films was determined to be 99 GPa and 92 GPa, respectively, which agrees reasonably well with the documented effective elastic modulus of bulk polycrystalline gold of 98 GPa. In addition, it was found that cracks on thin films had little effect on the determination of elasticity because the films were fully bonded and compliant to the substrates and the effect of cracks on the deformation of the substrate was small. The deformation of gold thin films was likely elastic as the strain experienced by the gold thin films during deformation was fairly small, less than 0.05%, even though gold is a very ductile metal. As

demonstrated by the result, the key equations of the theory (Eq. 4.5 and Eq. 4.12) on the applied load of the film fit well with each other ($R^2 > 0.97$) even though their formulations are completely different, suggesting the theory is consistent within itself.

Chapter 5
Polydopamine Thin Film as Bioadhesive

5.1 Introduction

Underwater adhesion is probably one of the most important benefits of bioadhesives. In the field of adhesion science, water or moisture has traditionally been treated as surface contaminants or weak boundary layers [98]. Synthetic adhesives perform poorly on wet surfaces or underwater due to a variety of complex mechanisms of deterioration including erosion, plasticization, swelling, and hydrolysis of the adhesive polymers [99]. Even though some may have strong bulk cohesive strength underwater, they fail eventually by the wicking and crazing of water due to poor interfacial adhesions with the adherends [100, 101]. Paradoxically, cells and most tissues in biology, with water comprising an average of 70% of their weight, are exquisitely assembled from adhesively bonded parts.

Water as a medium represents a completely different environment compared to in air. Non-covalent interactions are dramatically reduced in water due to the sheer abundance and strong electrostatic nature of water molecules [102]. Taking electrostatic interactions as an example, at a simplistic molecular level, Coulomb's law predicts that the interaction energy for two point charges is inversely proportional to the dielectric constant and the interionic distance. This means the interaction energy is 80 times weaker in water than in vacuum as the dielectric constant of water is 80 times higher than that of vacuum. In reality, this interaction energy is further diminished due to the increased interionic distance by the salvation effect or the local ordering of water molecules surrounding the charges. For instance, for two monovalent ions Na^+ and Cl^- in contact in vacuum, their energy of interaction is effectively reduced from about $200\ kT$ to only a few kT in water. Van der Waals interactions are penalized to a greater degree as their energies are inversely proportional to powers of the dielectric constant and the effect of dielectric constant on hydrogen bonds is basically unpredictable. In contrast, covalent interactions such as coordination bonds are largely unaffected providing the ligands of choice bind the metal more strongly than water [103] and hydrophobic interactions are enhanced by water.

Effective underwater adhesives can bring many utilities such as attaching sensors in ocean, repairing wet tissues, and patching leaky underwater oil pipelines. The objective of using bioadhesives for wet

applications, i.e. using Barnacle cements for the dental cements, has been pursued since at least the late 1960s [104]. During the last decade, new strategies for fabricating multi-functional bioadhesives were developed by exploiting the adhesive characteristics of DOPA, the key adhesion and crosslinking promoting catecholic residue identified in the adhesive proteins of mussels and sandcastle worms [7]. DOPA was coupled with poly(ethylene glycol) and glycine to create anti-fouling bioadhesives/coating that can anchor to different surfaces [105-108], functionalized on structured surfaces to build a reversible adhesive surface that works in both wet and dry conditions [15], and conjugated to poly(ethylene glycol) to form a medical hydrogel that immobilizes transplanted islets to epididymal fat pad and external liver surfaces [109, 110]. For underwater glues, polystyrene, which is not ordinarily a component of adhesives, was used to mimic mussel adhesive proteins by incorporating catechol side chains, for which the polymer displayed enhanced adhesion upon cross-linking [111]. In the same manner, the adhesive proteins of the sandcastle worm was also mimicked by synthesizing polyelectrolyte analogs with the same side chain chemistries and molar ratios of catechol, amine, and phosphate, forming a complex coacervate that qualitatively mimicked the entire range of natural glue behaviours including underwater delivery, interfacial adhesion, and triggered solidification [112-115]. Other biomimetic approaches include the expression of recombinant mussel adhesive proteins [116-118]. To date, the approaches mentioned above, although have successfully mimicked certain aspects of natural underwater glue in terms of fluid properties, solidification, and adhesion, none of them have displayed any practical performance, i.e. achieving significant bond strength within a reasonable curing time (< 2 hours). For instance, although the mimetic adhesive of sandcastle worm by Stewart *et al* have displayed a shear bond strength several times the estimated bond strength of the natural adhesive [115], the adhesive was applied on wet, smooth, and acid-treated aluminum substrates in air, and then submerged in water with a curing time of 24 hours.

In this study, we first extend our previous characterization of polydopamine thin films to wet conditions to gain insights on how to utilize polydopamine as a bioadhesive. Based on the understandings, we propose a fundamentally new strategy for fabricating underwater adhesive using polydopamine as the key ingredient. Our preliminary results showed that the new adhesive can bond to both hard and soft substrates in water as shown in Figure 5.1 and it can permanently bond macroscopically rough SEM standard aluminum stubs (12.7 mm in diameter) to glass slides in water

without pretreatments of either surfaces, obtaining an adhesive strength of 1 kg or half of that of natural adhesive within 2 hours of curing time.

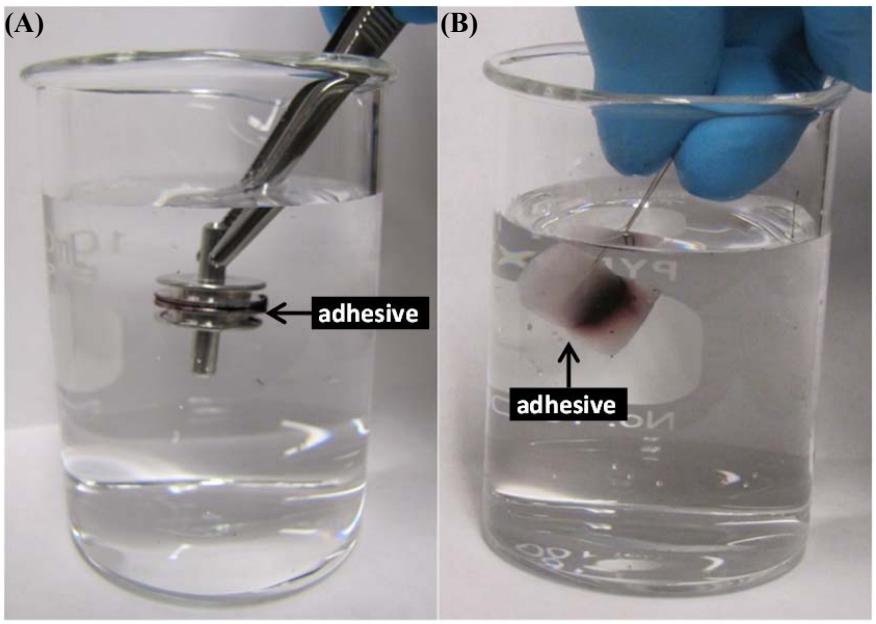

Figure 5.1: Photos of a pair of rigid aluminum SEM stubs (A) and two pieces of soft PVA hydrogels (B) joined by the dopamine-alginate hybrid hydrogel adhesive in 10 mM TRIS-HCl buffer at pH 8.5 for 2 hours of curing time. Note that the buffer solution was replaced by water for clarity.

5.2 Materials and Experimental

Dopamine hydrochloride was supplied by Sigma-Aldrich. TRIS-HCl buffer base (BP152) was supplied by Fisher BioReagents. Sodium alginate (Protanal HF 120 RBS) was supplied by FMC. Poly(dimethylsiloxane) (PDMS, Sylgard 170) was supplied by Dow Corning Corp., Midland, MI. Aluminum SEM stub (Product No: 16709) were supplied by TED PELLA, INC. Plain microscope slides were supplied by Fisher Scientific. Microscope slides and aluminum stubs were cleaned by acetone and deionized water before use. The opaque fillers in Sylgard 170 were removed by centrifugation and only the remaining clear solution was used. The cyanoacrylate-based commercial aquarium superglue, CorAffix gel, was supplied by Two Little Fishes, Inc.

5.2.1 Preparation of Flat Sheets and Hemispherical Tips of PDMS

The PDMS solution used for making elastomers was prepared by mixing the elastomer base and crosslinker at a weight ratio of 1:1. The flat sheet of PDMS was made by casting 2 mL of PDMS

solution onto a microscope slide and curing at 90°C for 2.5 hours. The sheet thickness was measured using an electronic digital caliper to be 1.25 ± 0.1 mm. The hemispherical tip of PDMS was made by first molding the PDMS solution into the hemispherical shape using a custom-made Teflon mold and then coating the resulting PDMS tip with a layer of PDMS solution to make the tip surface smooth. The tip core was cured at 90°C for 15 minutes and the tip coating along with the core was then cured at 90°C for 2.5 hours. The resulting tip radius was measured to be 3.0 ± 0.1 mm by analyzing the side-view image of the tip using a custom-written MATLAB (R2008a, MathWorks) script which gives a least squares best-fit to the curvature of the apex of the tip.

5.2.2 Coating Polydopamine Thin Films

The dopamine solution used for coating was made by dissolving dopamine hydrochloride at a concentration of 2 mg/mL in a 10mM TRIS-HCl buffer at pH 8.5. PDMS elastomers were submerged in the dopamine solution immediately for a period of 24 hours once the solution was made. To avoid the deposition of dopamine nanoparticles formed in the solution during the coating process, all samples of PDMS elastomers were placed upside down in the solution. The coated samples were dried in air or by pure nitrogen overnight.

5.2.3 Contact Angle Measurements of Polydopamine Thin Films

The static contact angles of a series of probe liquids on polydopamine coated PDMS substrates were measured by the sessile drop method, where a 5 μl drop of a probe liquid was dispensed onto the sample surface from a height of 2 cm at the room temperature in air. The side view image of the drop was recorded after the drop had stopped spreading (within 1 minute) and the contact angles were analyzed by a custom-made MATLAB script.

The Young equation is the most widely used method for determining the interfacial free energy between a liquid (l) and a solid (s) in an ambient atmosphere (v). When a liquid drop is placed on a flat solid surface, the energy of cohesion between the molecules of liquid is balanced by the energy of adhesion between the liquid and solid. The angle formed between the liquid-air (lv) interface and solid-liquid (sv) interface is known as the contact angle (θ), which arises from the thermodynamic equilibrium of the surface free energies (γ) at the solid-liquid (sl), liquid-air (lv), and solid-air (sv) interfaces [119]

$$\gamma_{sv} = \gamma_{sl} + \gamma_{lv} cos\theta \quad \text{Eq. 5.1}$$

Obtaining contact angles for a number of different liquids allow one to calculate the surface free energy (γ) of the solid consisting of the Lifshitz-van der Waals (γ^{LW}) apolar component and the electron donor (γ^{-}) electron acceptor (γ^{+}) acid-base (γ^{AB}) polar component, which include the hydrogen donor-hydrogen acceptor interactions [120], according to the van Oss' model [121]

$$\gamma = \gamma^{LW} + \gamma^{AB} \quad \text{Eq. 5.2}$$

$$\gamma^{AB} = 2\sqrt{\gamma^{+}\gamma^{-}}$$

Combining van Oss' model with the Young's equation, Eq. 5.1, we get

$$(1 + cos\theta)\gamma_{lv} = 2\left(\sqrt{\gamma_{sv}^{LW}\gamma_{lv}^{LW}} + \sqrt{\gamma_{sv}^{+}\gamma_{lv}^{-}} + \sqrt{\gamma_{sv}^{-}\gamma_{lv}^{+}}\right) \quad \text{Eq. 5.3}$$

Choosing more than three liquids with known surface free energy components enable one to determine the surface free components of the solid. The probe liquids included formamide, dimethyl sulfoxide (DMSO), elthylene glycol, diidomethane, glycerol and hexadecane. The contact angles of the probe liquids were cross-correlated with the contact angle of water as a pairing parameter, as advised by van Oss, to calculate the surface free energy of polydopamine.

5.2.4 Adhesive Pull-off Test by Micro-indenter

The micro-indentation system is comprised of a linear stage (Newport MFA-CC), a 25 gram force transducer (Transducer Techniques GS0-25), and an inverted optical microscope (Omano OMM300T) and controlled by a custom-written LabVIEW (version 8.5, National Instruments) program. The adhesive was directly injected and immediately sandwiched between a hemispherical PDMS tip and a microscope slide in TRIS-HCl buffered at pH 8.5 by loading the tip 50 μm down to the slide. After 12 hours of curing time, the tip was unloaded at 0.1 μm/s until the joint was broken. The force, displacement, time, and the bottom view of the contact area were recorded and analyzed.

5.2.5 Fabrication and Evaluation of Dopamine Alginate Hybrid Adhesive

The adhesive consisted of five readily available components and was utilized in two parts. The first part was a mixture of dopamine hydrochloride, TRIS, and ferric nitrate in deionized water at a mole

ratio of 12:96:1 for dopamine, water, and iron and a mass ratio of 2:1 for dopamine and TRIS. The second part was an aqueous solution containing 5 wt.% of sodium alginate. To join, 20 μL of the first part and 40 μL of the second parts were sequentially delivered to the joint such that the first part sandwiched the second. The adherends were firmly pressed together after each delivery to distribute the adhesive evenly at the joint. The joining was performed entirely in water where the adherends were fully submerged in a pH 8.5 buffer solution containing 10 mM TRIS-HCl at 28°C. After curing, the aluminum stubs were pulled vertically from the microscope slides at 10 mm/min using a Universal Material Tester (CETR) with a 1 kg load cell. The force and displacement information were recorded and analyzed and the broken joints were examined under a microscope.

5.2.6 XPS Study on Adhesive Joints

XPS spectra of the dehydrated joints were obtained using a Thermo Scientific K-Alpha analysis system (Leybold MAX20). A dual Mg/Al K_α anode operated at 216W was used for X-ray generation. Survey spectra were recorded for 0–1352 eV binding energy range, at a pass energy of 50 eV. High-resolution spectra of C1s, O1s, N1s, and Fe2p peaks were recorded at 20eV pass energy. To avoid sample degradation during analyses, exposure to X-ray radiation was limited by omitting high-resolution scans of low intensity peaks and recording scans only once. Spectral analysis was performed using the software supplied by the company (Avantage). Charge shift corrections were made by setting the C1s peak of saturated hydrocarbons to 285.0 eV. Peaks were fitted by fixing the full-width at half-maximum of the C1s, O1s, N1s, and Fe2p peaks at 1.75, 2.24, 1.56, and 3.37 eV, respectively, and setting the Gaussian/Lorentzian ratio to 30%. Three trials were completed for each sample.

5.3 Results and Discussion

5.3.1 Surface Free Energy of Polydopamine Thin Films

Static contact angle measurements were carried out on polydopamine coated PDMS substrate by the sessile drop method with formamide, DMSO, water, elthylene glycol, diidomethane, glycerol, and hexadecane as the probe liquids. The contact angles measured were analyzed according to van Oss' model, Eq. 5.3, with water as one of the pairing parameters to determine the surface free energy of polydopamine thin films. The results are present in Table 5.1. The Lifshiz-van der Waals component and the acid-base component of the surface free energy were determined to be $30\ \mathrm{mJ/m^2}$ and $10\ \mathrm{mJ/m^2}$, respectively. The values of the energy components are in good agreement with those

reported on polydopamine coated hydrophobic substrates [122], where the Lifshiz-van der Waals component ranges from 30 to 35 $\mathrm{mJ/m^2}$ and the acid-base component ranges from 5 to 15 $\mathrm{mJ/m^2}$.

The surface free energy provides fundamental understandings on the adhesion of polydopamine with different surfaces in water by examining the thermodynamic work of adhesion, which is the work required to split an interface into two and is equivalent to the energy difference between the surface free energy of the two surfaces and the initial interface. Based on van Oss' model [121], for splitting material 1 into two in vacuum and splitting material 1 and material 2 in vacuum and in medium 3, the corresponding work of adhesion (W) are

$$W_{11} = 2\gamma_1 \qquad \text{Eq. 5.4}$$

$$W_{12} = \gamma_1 + \gamma_2 - \gamma_{12} = 2\left(\sqrt{\gamma_1^{LW}\gamma_2^{LW}} + \sqrt{\gamma_1^{+}\gamma_2^{-}} + \sqrt{\gamma_1^{-}\gamma_2^{+}}\right) \qquad \text{Eq. 5.5}$$

$$W_{132} = \gamma_{13} + \gamma_{23} - \gamma_{12} = W_{12} + W_{33} - W_{13} - W_{23} \qquad \text{Eq. 5.6}$$

Using commercial SiO_2 covered glass as an example, assigning 41 $\mathrm{mJ/m^2}$, 62.4 $\mathrm{mJ/m^2}$, and 0 $\mathrm{mJ/m^2}$ to the Lifshiz-van der Waals (γ^{LW}), electron donor (γ^{-}), and electron acceptor (γ^{+}) energy components of glass [123], the work of adhesion between glass and polydopamine is 88.8 $\mathrm{mJ/m^2}$ in vacuum (Eq. 5.5) and -12.3 $\mathrm{mJ/m^2}$ in water (Eq. 5.6). The negative value indicates the interactions of polydopamine to surfaces in an aqueous medium must be a chemical one, presumably covalent, in order for bonding to occur, because the thermodynamic work of adhesion only accounts for reversible weak intermolecular interactions such as the van der Waals forces and the hydrogen bonds.

Table 5.1: Surface energy of polydopamine determined with one standard deviation based on contact angle measurements. The contact angles (θ) were obtained on polydopamine coated PDMS substrates using different liquids and were interpreted according to the acid-base theory of contact angles with water as one of the pairing parameter.

Liquid	γ^{LW} (mJ/m^2)	γ^{AB} (mJ/m^2)	γ^{+} (mJ/m^2)	γ^{-} (mJ/m^2)	γ (mJ/m^2)	θ (°) ± SD
Diidomethane	50.8	0.0	0	0	50.8	51.2 ± 2.6
DMSO	36	8.0	0.5	32	44	23.3 ± 1.9
Ethylene glycol	29	19.0	1.92	47	48	43.3 ± 1.2
Formamide	39	19.0	2.28	39.6	58	42.5 ± 2.6
Glycerol	34	30.0	3.92	57.4	64	67.2 ± 4.5

Hexadecane	27.5	0.0	0	0	27.5	16.4 ± 1.2
Water	21.8	51.0	25.5	25.5	72.8	64.8 ± 3.7
Polydopamine	30 ± 3.9	10 ± 5	1.4 ± 1.4	17.7 ± 4.3	40 ± 8.9	

5.3.2 Wet Adhesive Strength of Polydopamine

The adhesive strength of polydopamine was studied by in-situ polymerization of dopamine between two surfaces underwater. 0.1 mL of concentrated dopamine solution at 1:8 dopamine to water mole ratio was injected and sandwiched between a hemispherical soft PDMS tip and a flat rigid microscope slide in 10 mM TRIS-HCl buffer at pH 8.5. The soft tip was indented by 50 μm into the slide to ensure close contact between the two adherends while dopamine was being dissolved. The pull-off force was measured by unloading the tip from the slide at 0.1 μm/sec after 12 hours of curing time. Commercial aquarium superglue was used for control. As instructed by its user guide, the superglue was applied in air on wetted tip before loading the tip into the substrate in the buffer. Tests were also performed by injecting the superglue directly between the adherends in the buffer solution, but the adhesive strength was found to be much lower because the glue cures too fast. Figure 5.2A shows the typical load-displacement curves and Figure 5.2B shows the associated pull-off forces with one standard deviation. The pull-off force of 12 mN for the concentrated dopamine solution was significantly higher than the one for the commercial superglue at 0.3 mN, indicating bonding of polydopamine at the joint. The force translates to an adhesive strength of approximately 50 kPa accounting for the contact area, which was about 275 μm in radius.

Two problems of underwater joining were immediately apparent from the experiment. First, the test was repeated for 4 and 8 hours of curing time and the result indicated that the polymerization process of dopamine was too slow to be of any practical use: the test at 4 hours indicated a pull-off force less than 0.6 mN, which is statistically insignificant compared to our control and on the other hand, the joint at 8 hours was very unstable compared to the result at 12 hours and the pull-off force varied between 2 mN to 8 mN with a standard deviation of 4 mN. The slowness was also apparent from the coating process for which the film thickness is less than 5 nm after 2 hours of curing time [16, 23]. Second, the debonding process of the joint was instantaneous, as indicated by the almost vertical pull-off curve shown in the graph and by the abrupt disappearance of the contact area from observations. This shows that polydopamine was too rigid to resist peeling, the key mechanism of failure for macroscopic adhesion. The rigidness was consistent with the observations from the previous studies in Chapter 2 and Chapter 3 on the mechanical properties of polydopamine thin films.

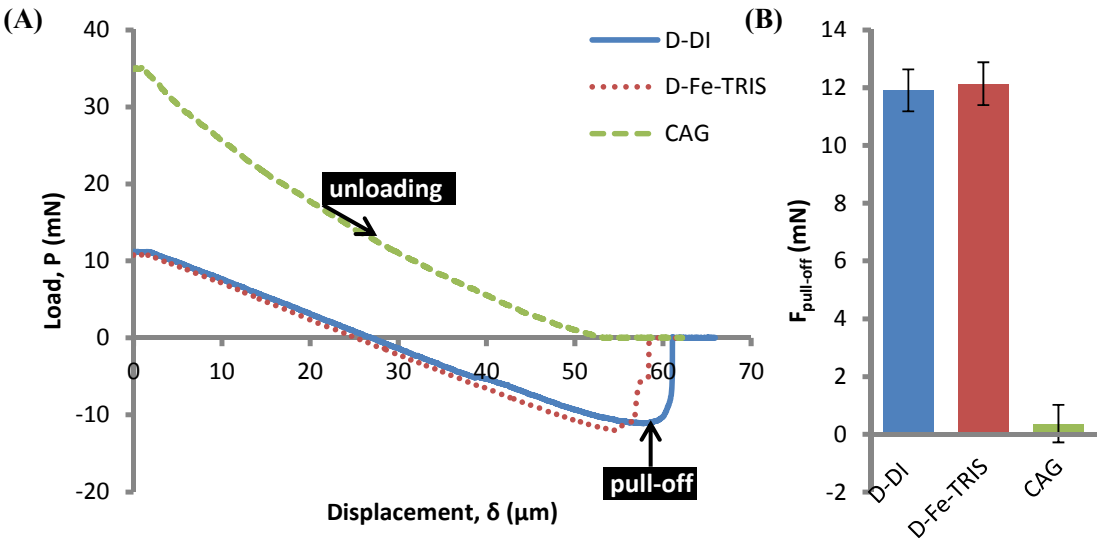

Figure 5.2: Typical load and displacement curves (A) and the associated pull-off forces with one standard deviation (B) of the concentrated dopamine solution (D-DI), the mixture of dopamine, TRIS, and ferric ion (D-Fe-TRIS), and the commercial aquarium superglue, CorAffix gel (CAG), joining hemispherical PDMS tips and flat glass slides in 10 mM TRIS-HCl buffer solution at pH 8.5. The joining was performed by sandwiching 0.1 mL of the adhesive between the tip and the slide at an indentation depth of 50 µm. After 12 hours of curing time, the pull-off was achieved by unloading the tip from the slide at 0.1 µm/s until separation.

To get around these problems, we propose to use dopamine as a crosslinker with ferric ions as the oxidant to accelerate the polymerization process and use alginate solution as the structural and adhesion support for the joint. The theoretical and experimental study has indicated that the bonding geometry of catechol strongly affects its molecular electronic structure [124]. In this respect, we suspect using small unbounded dopamine, due to increased molecular mobility of catechol, might be beneficial for joining compared to other strategies that employ large catecholic polymers [109-118].

5.3.3 Ferric Ion as Oxidant

The affinity of iron for catechol is established, a linear relationship was found to exist between the reduction potentials and the pH independent thermodynamic stability constants for the complex according to spectrophotometric data [125]. The oxidation of catechol and the reduction of ferric ion occur at similar potentials (~0.75 V) [126], allowing iron to interact with catechol via chelation, redox chemistry or a combination of both. Wilker *et al* observed a signal from an organic radical in the electron paramagnetic resonance spectrum of tris-Fe(DOPA-peptides)$_3$ [127, 128] and proposed a

model that suggests a semiquinone radical is formed by the coupled reduction of ferric ion and the oxidation of DOPA for which the reaction of the semiquinone radical with oxygen forms a second radical that can participate in the covalent crosslinking or bonding to an interface [129]. The model explains why ferric ion induced significantly more cross-linking than other metal ions or simple oxidants [130].

In our experiment, we formed a complex mixture of dopamine hydrochloride, TRIS, and ferric nitrate in deionized water at a mole ratio of 12:96:1 for dopamine, water, and iron and a mass ratio of 2:1 for dopamine and TRIS. The mixture displayed an intense dark red color indicating strong charge transfer from the non-bonding π orbitals of catechol oxygen to empty *d* orbitals of iron [131]. It appeared to be fairly stable as it showed no visible changes in viscosity or in color within 6 hours after creation. However, upon exposure to a large quantity of TRIS buffer, the mixture precipitated and behaved rheologically like viscous particle dispersion that spreads and "wets" surfaces. Exposing the precipitates to buffer over time (more than 12 hours) caused them to crosslink forming a weak 3 dimensional gel network that was able to hold its own weight. This precipitation of dopamine-iron has been reported in literature [132] and is consistent with Wilker's model. However, the cause for the stability of the concentrated complex mixture is unknown.

It was reported recently that according to *in situ* resonance Raman spectroscopy, the iron coordination chemistry increases the crosslink density of proteins in the outer cuticle of the byssal threads of mussels, responsible for their high hardness and high extensibility [133]. Several other studies have reported that ferric ions increase the cross-linking between catechol functional groups [134, 135]. In particular, a self-healing polymer network was formed by the catechol-iron chemistry and the gel showed an elastic modulus approaching that of covalently cross-linked gels [136]. Conversely, none of the mechanical changes mentioned above was detected in our study; the iron-dopamine complex mixture was tested for wet adhesive strength and the result was not different from concentrated dopamine solution, as shown in Figure 5.2A. This is probably because the iron concentration at the joint was much lower than the dopamine concentration such that the iron-dopamine coordination structure was overwhelmed by the random self-polymerization of dopamine, as indicated by our XPS data mentioned in the next subsection.

5.3.4 Structure and Performance of Dopamine Alginate Hybrid Adhesive

5 wt. % alginate solution was used in conjunction with the dopamine-iron complex mixture to provide structural and rheological support. It is expected to deliver temporary adhesion and cohesion at the joint because of its high viscosity, the result of hydrogen bonding among the carboxylic and hydroxyl functional groups of alginate. Alginate is known to gel in the presence of multivalent ions [137]. We name this combination "dopamine alginate hybrid adhesive".

Standard aluminum SEM stubs was joined to microscope slides by sequent injections of the complex mixture and the alginate solution at the joint in the buffer solution at pH 8.5, such that the mixture sandwiches the solution at the interface. Figure 5.3 compares the pull-off forces of the joints at different curing times. The pure iron solution in combination with alginate and the commercial superglue were used as controls. Again, the commercial superglue was applied to wet SEM stub surface in air while both the bioadhesive and the pure iron control were applied directly underwater.

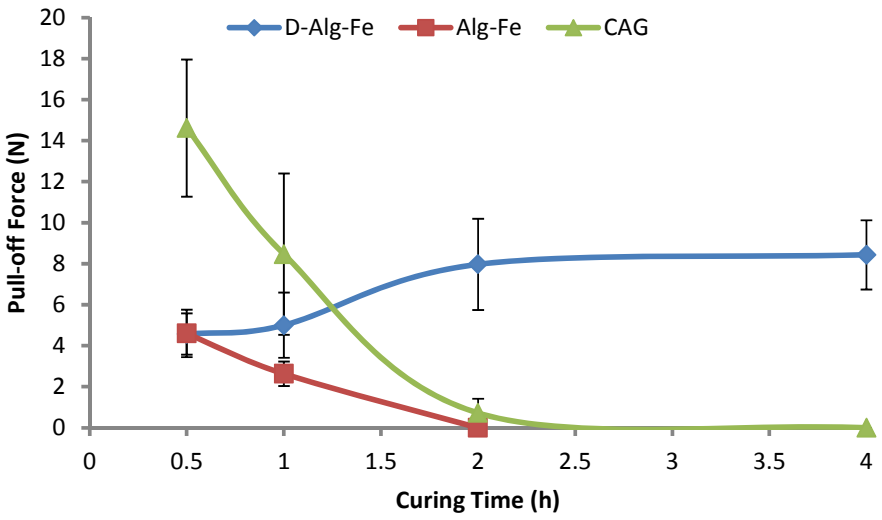

Figure 5.3: Comparison of pull-off forces of the dopamine-alginate hybrid hydrogel adhesive (D-Alg-Fe), the adhesive without dopamine (Alg-Fe), and the commercial aquarium superglue, CorAffix gel (CAG) joining aluminum SEM stubs on flat glass slides in 10 mM TRIS-HCl buffer solution at pH 8.5 and 28°C. The D-Alg-Fe and Alg-Fe were applied directly underwater while the CAG was deposited on wet surface in air before immersed underwater.

The results showed that although the hybrid adhesive and its pure iron control both have the same initial pull-off force of 5 N at 30 min curing time, the force for the hybrid adhesive increased over

time and plateaued at 10 N for 2 hours of curing time while the force for the control diminished to zero within 2 hours. Accounting for the contact area of the SEM stub of 127 mm^2, 10 N translates to 80 kPa, which is about half of that of natural mussel adhesion to glass at 171 kPa [138]. It should be noted that the actual strength of the adhesive is likely higher as the surface of the SEM stubs displayed a macroscopic roughness that was visible to the naked eye. The joint of hybrid adhesive appeared to be permanent as it remained intact in fresh deionized water within the observation period of 3 months. The failure of the joint was cohesive under the examination of microscope indicating bonding at both surfaces. In comparison, the commercial superglue cured and hardened faster (in 5 min) in the buffer and displayed a much stronger initial adhesion of 15 N than our adhesive, but it quickly lost its strength and the pull-off force was only around 1 N at 2 hours of curing time. The failure of the joint for CAG was adhesive at the glue-glass interface and was likely a result of crazing of water at the interface as reported by many others [2]. Tests were repeated for the case of pure dopamine and pure dopamine-iron complex and no pull-off forces were detected for these. We attribute the exceptional performance of the hybrid adhesive to the combination of the immediate cohesion of alginate and the gradual adhesion of dopamine.

The structure of the hybrid adhesive was investigated by XPS. Broken joints were dried in pure nitrogen or in air and then tested. However, it was found that we could not detect iron content in the joint. Since we are most interested in the coordination chemistry of iron, hybrid adhesive samples were made with higher iron content (at a mole ratio to dopamine of 1:8 instead of 1:12) by depositing 0.1 mL of the iron complex mixture on 0.1 mL of the alginate solution on a glass slide in air, then immediately submerging the sample in buffer for 24 hours, and afterwards drying the resulting gel in pure nitrogen overnight before sending the sample for XPS analysis. The pure iron solution control, the pure alginate, and the polydopamine coated PDMS substrate were also tested for comparison. The results are shown in Figure 5.4. Although the surface of the hybrid adhesive samples was most covered by dopamine-iron, the high resolution scans of O_{1s} revealed that the spectra for hybrid adhesive in Figure 5.4C was a combined outcome of alginate-Fe hydrogel in Figure 5.4D and polydopamine in Figure 5.4B suggesting polydopamine and alginate were present in the hybrid adhesive. The O/C atomic ratio of alginate-Fe hydrogel in Figure 5.4E was significantly higher than pure alginate. The excessive oxygen was most likely due to the complexation of hydroxide ions in the buffer to iron ion. In comparison, the O/C ratio for the hybrid hydrogel was significantly lower than the ratio for pure alginate and was similar to polydopamine suggesting the hydroxide ligands were

replaced by dopamine. The atomic composition of the hybrid adhesive in Table 5.2 revealed that the ratio between dopamine and iron was approximately 16:1, which was significantly higher than the initial 8:1 ratio. This can be explained by Wilker's model and his experimental studies [128, 129] which indicate that radicals only form in tris Fe(DOPA-peptide)$_3$ not in mono Fe(DOPA-peptide) or bis Fe(DOPA-peptide)$_2$. This means that the precipitates of iron-dopamine tend to form where dopamine is the most concentrated and hence, the dopamine concentration was higher at the joint than its initial concentration relative to the concentration of iron.

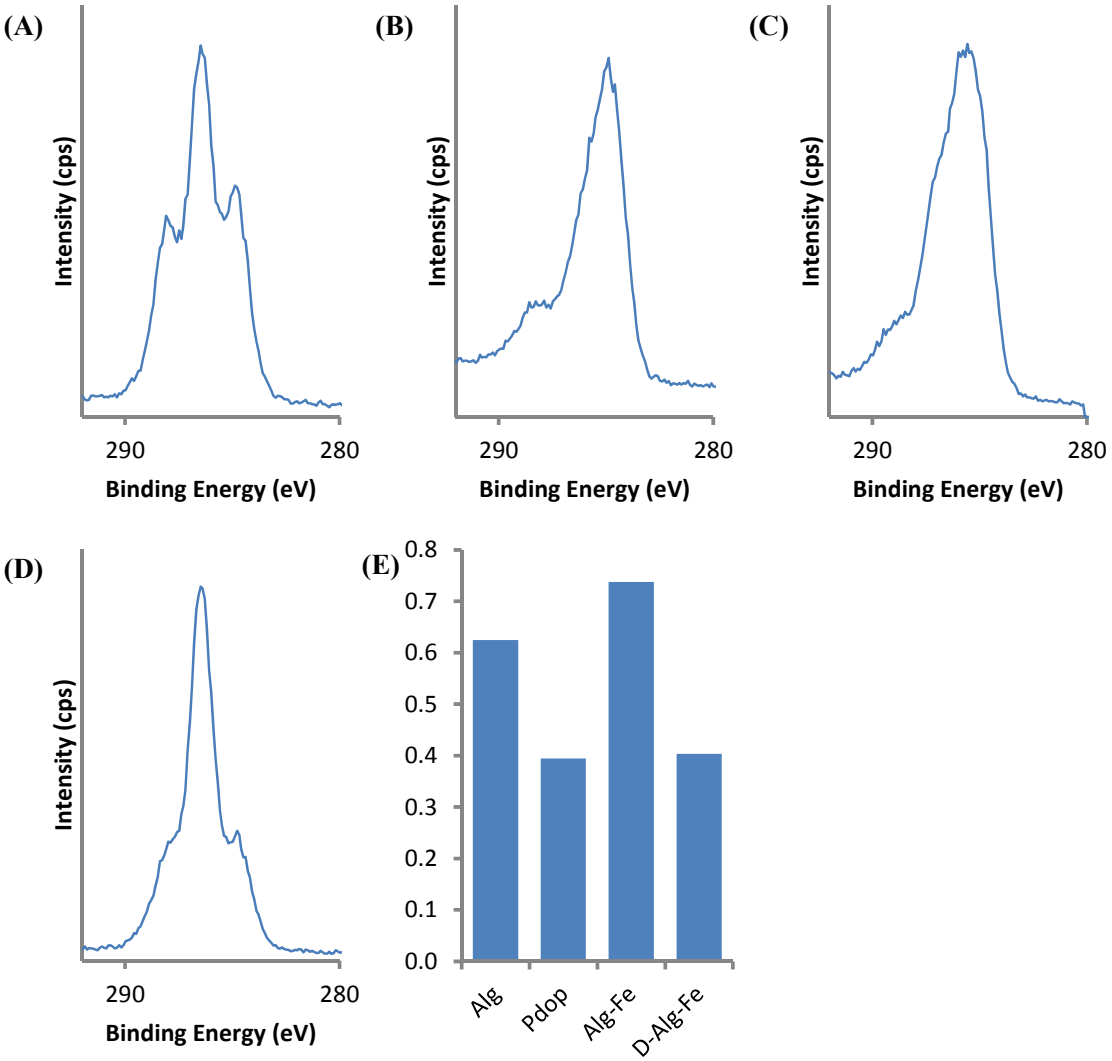

Figure 5.4: Comparison of the O_{1s} peaks of the XPS spectrum of pure alginate (Alg; A), polydopamine thin film (Pdop; B), dopamine-alginate hybrid hydrogel (D-Alg-Fe; C), and alginate-Fe hydrogel (Alg-Fe; D) at high resolution and their O/C ratios (E).

The interactions between dopamine and alginate were investigated by comparing the flow of alginate solutions made with TRIS buffer with and without dopamine (at 2 mg/mL) after a waiting period of 24 hours. Even though the color of the sample with dopamine had turned to dark black from bright orange due to the polymerization of dopamine, there were no indications that the viscosity of the sample with dopamine is higher. This means the interactions were rather weak. From a chemistry perspective, dopamine is known to form covalent bonds with amino and thiol functional groups via

Michael addition and Schiff base reactions [13, 14], but none of these functional groups were present in alginate. Hence, we suspect the connection between dopamine and alginate in the hybrid adhesive was through the bridging of iron and we propose the following mechanism, which is demonstrated in Figure 5.5.

Table 5.2: Surface chemical composition of pure alginate, polydopamine thin film, polydopamine-alginate-Fe hydrogel, and alginate-Fe hydrogel.

at.%	C1s	N1s	O1s	Fe2p3
Alg	60.6	1.6	37.8	
Pdop	66.9	6.7	26.4	
Alg-Fe	54.5	3.7	40.2	1.6
Pdop-Alg-Fe	66.2	6.6	26.7	0.5

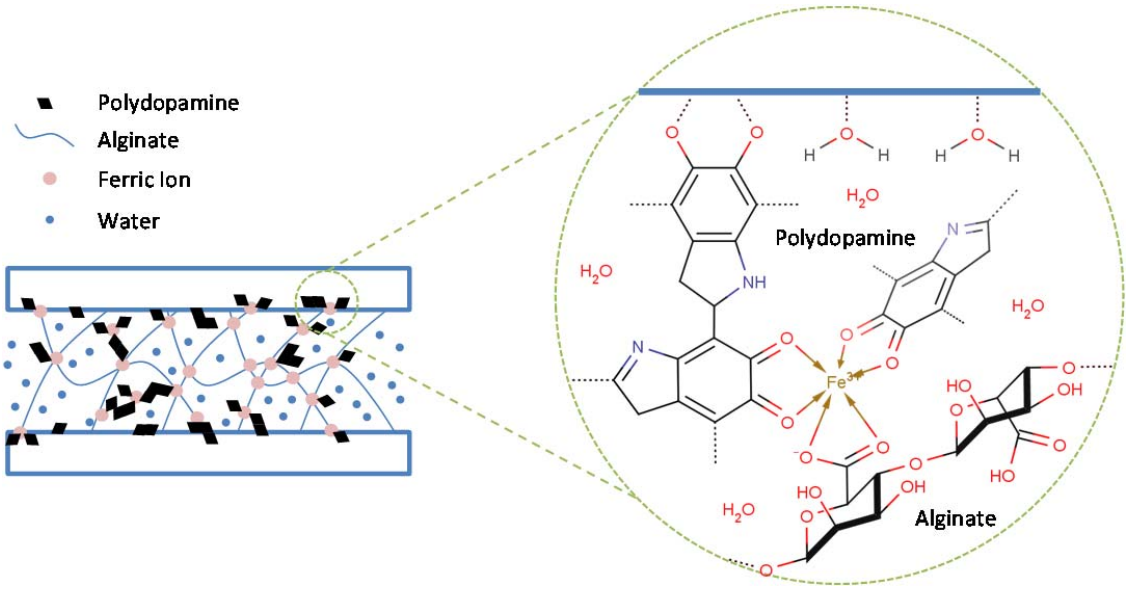

Figure 5.5: Conceptual illustration of the joint formed using dopamine-alginate hybrid hydrogel adhesive. The zoomed view shows the supposed molecular interactions between the components, namely, the coordination bonds between the catechol functional group of dopamine with the ferric ion, the ionic bonds between the alginate and the ferric ion, the self-polymerization of dopamine, and the chemical bonding of polydopamine to the adherend's surface through its catechol functionality.

The dopamine alginate hybrid adhesive represents a fundamentally different approach to the fabrication of underwater adhesives. In this approach, dopamine and its oxidant, iron, were used as crosslinkers to alginate polymers. To date, all other approaches have been focusing on mimicking natural underwater glue proteins by conjugating catechol functionalities to long-chain polymers [111-118]. None of the bioadhesives by these approaches have reached the same practical performance as ours. We believe this is partially because our approach has avoided one of the biggest engineering dilemmas faced in the bioadhesive research, that is, when catechol functional groups are part of the adhesive polymers, they affect not only the adhesion and crosslinking aspects but also the physical behaviours such as structures and fluid characteristics of the adhesive. If the interactions among the catechol functional groups are too strong, the adhesive will solidify too quickly in water and fail to establish contact with the adherends and in contrast, if the interactions are too weak, the adhesive will fail to perform. Consequently, the balance between the adhesion and the physical behaviour of the adhesive becomes an intricate matter, adding complexity to the problem of underwater adhesion. Most of the recent researches were dedicated to solving this problem through complex coacervation [113, 115, 118, 139], which is a process in which aqueous solutions of polyanions and polycations undergo phase separation at a pH which they electrically neutralize each other. The denser and smaller phase is polymer rich and has characteristics such as phase-separated fluidity, reduced viscosity, low interfacial energy, and high internal protein and solvent diffusion coefficient that are ideal for underwater adhesion. As tempting and elegant this solution might sound, we do not believe that we have to go through this complexity. Moreover, it is too early to speculate on the details of how marine organisms practice coacervation [139].

5.4 Conclusions

Two types of experiments were performed on polydopamine coated on or bonded between inorganic and polymer substrates. Contact angle measurements were carried out on polydopamine coated PDMS substrate by the sessile drop method with six different probe liquids. The results were analyzed according to van Oss' model with water as one of the pairing parameters, revealing a Lifshiz-van der Waals component and an acid-base component of surface free energy of polydopamine of $30\ \mathrm{mJ/m^2}$ and $10\ \mathrm{mJ/m^2}$. The surface energy components indicate that the interactions of polydopamine to surfaces in an aqueous medium must be a chemical one for adhesion to occur. The wet adhesive strength of polydopamine was studied by the in-situ polymerization of dopamine between a PDMS surface and a glass surface underwater and the subsequent pull-off of the

adherends after 12 hours of curing time. The pull-off force of polydopamine revealed an adhesive strength of approximately 50 kPa, indicating bonding of polydopamine at the joint. The adhesion characteristics of polydopamine indicated that the bonding was too slow and too rigid for practical applications. Based on the understanding, we proposed a new strategy for building underwater adhesive which utilizes polydopamine as a cross-linker for alginate solution. The hybrid adhesive combines the gradual adhesion of dopamine with the immediate cohesion of alginate with iron ions as the oxidant and the bridging element. The preliminary results of the adhesive demonstrate better practical performances than other studies; the adhesive was able to produce a permanent tensile adhesive strength of 80 kPa joining aluminum and glass with macroscopic roughness at the interface within 2 hours of curing time.

Chapter 6
Summary and Recommendation

6.1 Summary

Three consecutive studies were carried out to derive fundamental insights into the adhesion properties of polydopamine thin films.

(i) Characterization of the adhesion properties.

Three types of experiments (water contact angle, contact adhesion, and adhesive bonding) had been performed to investigate the adhesion behaviour of polydopamine thin films coated on or bonded between inorganic and polymer substrates. Polydopamine-coated polydimethylsiloxane surface had a static contact angle of 65°, suggesting a complete surface coverage by a layer of polydopamine. Wettability of the polydopamine-coated surface was further characterized by dynamic water contact angle measurements, revealing a large contact angle hysteresis of about 60° between the advancing and receding angles. The low receding contact angle suggested the formation of a hydration layer when exposed to water. Polydopamine-coated surfaces in air are relatively inert and have a low self-adhesion compared with the uncoated PDMS surfaces, reflecting the non-conformal, glassy nature of the polydopamine layer. The asymmetric contact between the polydopamine-coated surface and PDMS surface showed the highest adhesion force and hysteresis. The dopamine solutions was found able to bond two rigid surfaces (Al and glass) and the adhesive bonding strength increased with the amount of dopamine and saturated at 5 mg/ml. The direct joining of Al and PDMS using dopamine solution was challenging because of the hydrophobic nature of PDMS; a pre-coating of dopamine on PDMS was found useful. There were no significant bonding strength enhancements in the PDMS/Al system. In conclusion, this study in elucidating the surface and adhesion behaviour of polydopamine revealed that dopamine is able to coat plastic, ceramic and metal surfaces, and join or bond rigid substrates but might not be suitable for joining soft or flexible parts as polydopamine films are glassy.

(ii) Investigation of the mechanical properties.

Two types of experiments (crack formation and contact deformation) had been performed on polydopamine thin films coated on soft PDMS substrates to investigate the performance of polydopamine as an adhesive joint. Observations from the drying process suggest that the

polydopamine thin film is a layer of gel which shrinks if dehydrated. Extra attentions should be paid if polydpamine thin film is used as a composite material, i.e. a sub-layer of a membrane, as the shrinkage of the film can introduce undesired residual stresses to the system. The contact deformation study showed that the polydopamine thin film was strongly bonded to the substrate and was fairly robust as it complied fully with the deformation of the substrate during indentation and stood intact after repeat indentations. Analyzing the contact deformation in the framework of JKR and thin film contact mechanics revealed an effective elastic modulus of 7 GPa for polydopamine. In conclusion, it is recommended to coat/joint polydopamine with substrates stiffer than 7 GPa as anything softer would make polydopamine prone to cracking, undermining its integrity and it is not recommended to dry polydopamine for any applications unless drying is absolutely necessary. In this study, we were able to extend the JKR theory to accommodate the deformation of polydopamine thin films (100 nm thick), obtaining their elasticity by incorporating the plate theory into contact mechanics. The extended theory was termed the "thin film contact mechanics" and was validated against the contact deformation of gold thin films of two different thicknesses, 50 nm and 100 nm, sputtered on soft PDMS substrates at the room temperature. It was found that the theory was self-consistent and predicted the elastic properties of gold thin films fairly well. The effective elastic modulus of gold thin films was determined to be 99 GPa and 92 GPa, respectively, which agrees reasonably well with the documented effective elastic modulus of bulk polycrystalline gold of 98 GPa. In addition, it was found that cracks on thin films had little effect on the determination of elasticity because the films were fully bonded and compliant to the substrates and the effect of cracks on the deformation of the substrate was small. The deformation of gold films were likely elastic as the strain experienced by the gold thin films during deformation were fairly small, less than 0.05%, even though gold is a very ductile metal.

(iii) Exploration of the potential of polydopamine as a wet adhesive.

Two types of experiments (contact angle and wet adhesion) were performed on polydopamine coated on or bonded between inorganic and polymer substrates. Contact angle measurements were carried out on polydopamine coated PDMS substrate by the sessile drop method with six different probe liquids. The results were analyzed according to van Oss' model with water as one of the pairing parameters, revealing a Lifshiz-van der Waals component and an acid-base component of surface free energy of polydopamine of $30\ \mathrm{mJ/m^2}$ and $10\ \mathrm{mJ/m^2}$, respectively. The result indicates the interactions of polydopamine to surfaces in an aqueous medium must be a chemical one for adhesion

to occur. The wet adhesive strength of polydopamine was studied by in-situ polymerization of dopamine between a PDMS surface and a glass surface underwater and the subsequent pull-off of the adherends after 12 hours of curing time. The pull-off force of polydopamine revealed an adhesive strength of approximately 50 kPa, indicating bonding of polydopamine at the joint. The wet adhesion characteristics of polydopamine revealed that the bonding was too slow and too rigid for practical applications. Based on the understanding, we proposed a new strategy for building underwater adhesive which utilizes polydopamine as a cross-linker for alginate solution. The hybrid adhesive combines the gradual adhesion of dopamine with the immediate cohesion of alginate with iron ions as the oxidant and the bridging element. The preliminary results of the adhesive demonstrate better practical performances than other studies; the adhesive was able to produce a permanent tensile adhesive strength of 80 kPa joining aluminum and glass with macroscopic roughness at the interface within 2 hours of curing time.

6.2 Recommendation

For future work, the following recommendations are suggested:

(i) In dynamic water contact angle measurements, polydopamine thin film displayed a large contact angle hysteresis of about 60° between the advancing and receding angles. Although two plausible explanations, the presence of hydrophilic functional groups and the absorption of liquid, for this were proposed, the amount of contribution from each mechanism is uncertain. Measurements at different liquid dispensing rates might be used to gain some insights on this.

(ii) The derivation of the thin film contact mechanics employs a force balance that connects the JKR contact mechanics with the plate theory. The relation might be more concrete if it is presented from an energy perspective.

(iii) For validating the thin film contact mechanics, only two thicknesses of gold thin films, 50 nm and 100 nm, were tested, for which the elastic modulus of the film is expected to be and was consistent with the modulus of the bulk. Nevertheless, it would be interesting to extend the study to 10 nm gold thin films as the modulus is expected to be different from the bulk due to the presence of interfacial (between the film and substrate) and surface forces.

(iv) Thin film contact mechanics was applied to investigate the effective elastic modulus of dried polydopamine thin films. It would be worth trying to apply the technique to wet polydopamine thin

films to demonstrate the capability of the technique. To do so, a better microscope for viewing the contact area is required. In the same principle as nano-indentation, we should be able extend the technique to probe the plastic deformation of the film by increasing the tip elasticity or decreasing the tip radius.

(v) The mixture of dopamine and iron ions precipitated and behaved rheologically like viscous particle dispersion that spreads and "wets" surfaces upon exposure to a large quantity of buffer solution. The science behind the transition is unclear and it should be further investigated to gain some fundamental insights on the complex chemistry. In addition, different material compositions of the dopamine-hydrogel hybrid adhesive should be tested to make the study more comprehensive.

Appendix A
List of Publications

Journal

[1] F. K. Yang and B. Zhao, "Adhesion properties of self-polymerized dopamine thin film," *Surface Science*, pp. 115-122, 2011.

[2] F. K. Yang, W. Zhang, and B. Zhao, "Thin film contact mechanics," In preparation, 2011.

[3] F. K. Yang and B. Zhao, "Polydopamine hydrogel hybrid adhesive," In preparation, 2011.

Conference Proceeding

[1] Y. Han, F. K. Yang, H.J. Kwon, and B. Zhao, "Contact dynamics characterization of polymer thin films using a JKR-type apparatus," *International Conference on Nanotechnology: Fundamental and Applications*, 2011.

Patent

[1] F. K. Yang, and B. Zhao, "Composition, Methods, Applications of Underwater Adhesive or "Superglue", Provisional application filed [61/629,789], 2011.

Bibliography

[1] A. Higgins, “Adhesive bonding of aircraft structures,” *International Journal of Adhesion and Adhesives*, vol. 20, no. 5, pp. 367–376, 2000.

[2] A. J. Kinloch, “Review: The science of adhesion Part 1 Surface and interfacial aspects,” *Journal of Materials Science*, vol. 15, pp. 2141-2166, 1980.

[3] Smith, A.M. & Callow, J.A., eds. (2006) *Biological Adhesives.* Springer, Berlin.

[4] J. Waite, “Nature’s underwater adhesive specialist,” *International Journal of Adhesion and Adhesives*, vol. 7, no. 1, pp. 9-14, Jan. 1987.

[5] M. Wiegemann, “Adhesion in blue mussels (Mytilus edulis) and barnacles (genus Balanus): Mechanisms and technical applications,” *Aquatic Sciences*, vol. 67, no. 2, pp. 166-176, May. 2005.

[6] R. A. Jensen and D. E. Morse, “The bioadhesive of Phragmatopoma californica tubes: a silk-like cement containing L-DOPA,” *Journal of Comparative Physiology B: Biochemical, Systemic, and Environmental Physiology*, vol. 158, no. 3, pp. 317–324, 1988.

[7] J. H. Waite and M. L. Tanzer, “Polyphenolic substance of Mytilus edulis: novel adhesive containing L-Dopa and hydroxyproline,” *Science (New York, N.Y.)*, vol. 212, no. 4498, pp. 1038-40, May. 1981.

[8] M. Yu, J. Hwang, and T. J. Deming, “Role of l -3,4-Dihydroxyphenylalanine in mussel adhesive proteins,” *Journal of the American Chemical Society*, vol. 121, no. 24, pp. 5825-5826, Jun. 1999.

[9] H. Lee, N. F. Scherer, and P. B. Messersmith, “Single-molecule mechanics of mussel adhesion.,” *Proceedings of the National Academy of Sciences of the United States of America*, vol. 103, no. 35, pp. 12999-3003, Aug. 2006.

[10] B. A. Borgias, S. R. Cooper, Y. B. Koh, and K. N. Raymond, “Synthetic, structural, and physical studies of titanium complexes of catechol and 3, 5-di-tert-butylcatechol,” *Inorganic Chemistry*, vol. 23, no. 8, pp. 1009–1016, Nov. 1984.

[11] J. Moser, S. Punchihewa, P. P. Infelta, and M. Graetzel, "Surface complexation of colloidal semiconductors strongly enhances interfacial electron-transfer rates," *Langmuir*, vol. 7, no. 12, pp. 3012-3018, 1991.

[12] C. L. Frye, "Pentacoordinate silicon derivatives. IV. Alkylammonium siliconate salts derived from aliphatic 1,2-diols," *Journal of the American Chemical Society*, vol. 92, no. 5, pp. 1205-1210, 1970.

[13] M. J. LaVoie, B. L. Ostaszewski, A. Weihofen, M. G. Schlossmacher, and D. J. Selkoe, "Dopamine covalently modifies and functionally inactivates parkin," *Nature Medicine*, vol. 11, no. 11, pp. 1214–1221, 2005.

[14] L. A. Burzio and J. H. Waite, "Cross-linking in adhesive quinoproteins: studies with model decapeptides," *Biochemistry*, vol. 39, no. 36, pp. 11147–11153, 2000.

[15] H. Lee, B. P. Lee, and P. B. Messersmith, "A reversible wet/dry adhesive inspired by mussels and geckos," *Nature*, vol. 448, no. 7151, pp. 338-41, Jul. 2007.

[16] H. Lee, S. M. Dellatore, W. M. Miller, and P. B. Messersmith, "Mussel-inspired surface chemistry for multifunctional coatings," *Science (New York, N.Y.)*, vol. 318, no. 5849, pp. 426-30, Oct. 2007.

[17] R. A. Wise, "Dopamine, learning and motivation," *Nature Reviews Neuroscience*, vol. 5, no. 6, pp. 483–494, 2004.

[18] W. Montagna, G. Prota, J. A. Kenney Jr., *Black Skin: Structure and Function*. Academic Press, San Diego, CA, 1993.

[19] F. Bernsmann et al., "Characterization of dopamine−melanin growth on silicon oxide," *The Journal of Physical Chemistry C*, vol. 113, no. 19, pp. 8234-8242, May. 2009.

[20] J. Riesz, J. Gilmore, and P. Meredith, "Quantitative scattering of melanin solutions," *Biophysical Journal*, vol. 90, no. 11, pp. 4137–4144, 2006.

[21] P. Meredith, B. J. Powell, J. Riesz, S. P. Nighswander-Rempel, M. R. Pederson, and E. G. Moore, "Towards structure–property–function relationships for eumelanin," *Soft Matter*, vol. 2, no. 1, pp. 37–44, 2005.

[22] E. Kienzl, L. Puchinger, K. Jellinger, W. Linert, H. Stachelberger, and R. F. Jameson, "The role of transition metals in the pathogenesis of Parkinson's disease," *Journal of the Neurological Sciences*, vol. 134, pp. 69–78, 1995.

[23] F. Bernsmann et al., "Dopamine-melanin film deposition depends on the used oxidant and buffer solution," *Langmuir : the ACS journal of surfaces and colloids*, Feb. 2011.

[24] H. Lee, Y. Lee, A. R. Statz, J. Rho, T. G. Park, and P. B. Messersmith, "Substrate-independent layer-by-layer assembly by using mussel-adhesive-inspired polymers," *Advanced Materials*, vol. 20, no. 9, pp. 1619-1623, May. 2008.

[25] H. Lee, J. Rho, and P. B. Messersmith, "Facile conjugation of biomolecules onto surfaces via mussel adhesive protein inspired coatings," *Advanced materials (Deerfield Beach, Fla.)*, vol. 21, no. 4, pp. 431-434, Jan. 2009.

[26] S. Kang and M. Elimelech, "Bioinspired single bacterial cell force spectroscopy," *Langmuir : the ACS journal of surfaces and colloids*, vol. 25, no. 17, pp. 9656-9, Sep. 2009.

[27] R. Ouyang, J. Lei, and H. Ju, "Artificial receptor-functionalized nanoshell: facile preparation, fast separation and specific protein recognition," *Nanotechnology*, vol. 21, no. 18, p. 185502, May. 2010.

[28] W. Ye, D. Wang, H. Zhang, F. Zhou, and W. Liu, "Electrochemical growth of flowerlike gold nanoparticles on polydopamine modified ITO glass for SERS application," *Electrochimica Acta*, vol. 55, no. 6, pp. 2004-2009, Feb. 2010.

[29] W. H. Zhou, S. F. Tang, Q. H. Yao, F. R. Chen, H. H. Yang, and X.-R. Wang, "A quartz crystal microbalance sensor based on mussel-inspired molecularly imprinted polymer," *Biosensors & bioelectronics*, vol. 26, no. 2, pp. 585-589, Jul. 2010.

[30] A. Postma, Y. Yan, Y. Wang, A. N. Zelikin, E. Tjipto, and F. Caruso, "Self-polymerization of dopamine as a versatile and robust technique to prepare polymer capsules," *Chemistry of Materials*, vol. 21, no. 14, pp. 3042-3044, Jul. 2009.

[31] S. H. Ku, J. S. Lee, and C. B. Park, "Spatial control of cell adhesion and patterning through mussel-inspired surface modification by polydopamine," *Langmuir : the ACS journal of surfaces and colloids*, vol. 26, no. 19, pp. 15104-8, Oct. 2010.

[32] S. H. Ku, J. Ryu, S. K. Hong, H. Lee, and C. B. Park, "General functionalization route for cell adhesion on non-wetting surfaces," *Biomaterials*, vol. 31, no. 9, pp. 2535-41, Mar. 2010.

[33] J. Cui, Y. Wang, A. Postma, J. Hao, L. Hosta-Rigau, and F. Caruso, "Monodisperse polymer capsules: tailoring size, shell thickness, and hydrophobic cargo loading via emulsion templating," *Advanced Functional Materials*, vol. 20, no. 10, pp. 1625-1631, May. 2010.

[34] B. Fei et al., "Coating carbon nanotubes by spontaneous oxidative polymerization of dopamine," *Carbon*, vol. 46, no. 13, pp. 1795-1797, Nov. 2008.

[35] S. Ben-Valid, B. Botka, K. Kamarás, A. Zeng, and S. Yitzchaik, "Spectroscopic and electrochemical study of hybrids containing conductive polymers and carbon nanotubes," *Carbon*, vol. 48, no. 10, pp. 2773-2781, Aug. 2010.

[36] H. Hu, B. Yu, Q. Ye, Y. Gu, and F. Zhou, "Modification of carbon nanotubes with a nanothin polydopamine layer and polydimethylamino-ethyl methacrylate brushes," *Carbon*, vol. 48, no. 8, pp. 2347-2353, Jul. 2010.

[37] W. Ye, H. Hu, H. Zhang, F. Zhou, and W. Liu, "Multi-walled carbon nanotube supported Pd and Pt nanoparticles with high solution affinity for effective electrocatalysis," *Applied Surface Science*, Apr. 2010.

[38] M. Zhang, X. Zhang, X. He, L. Chen, and Y. Zhang, "Preparation and characterization of polydopamine-coated silver core/shell nanocables," *Chemistry Letters*, vol. 39, no. 6, pp. 552-553, 2010.

[39] F. Bernsmann et al., “Use of dopamine polymerization to produce free-standing membranes from (PLL-HA)n exponentially growing multilayer films,” *Soft Matter*, vol. 4, no. 8, p. 1621, 2008.

[40] B. Li, W. Liu, Z. Jiang, X. Dong, B. Wang, and Y. Zhong, “Ultrathin and stable active layer of dense composite membrane enabled by poly(dopamine),” *Langmuir : the ACS journal of surfaces and colloids*, vol. 25, no. 13, pp. 7368-74, Jul. 2009.

[41] J. Ou, J. Wang, S. Liu, J. Zhou, and S. Yang, “Self-Assembly and tribological property of a novel 3-layer organic film on silicon wafer with polydopamine coating as the interlayer,” *The Journal of Physical Chemistry C*, vol. 113, no. 47, pp. 20429-20434, Nov. 2009.

[42] Z. Y. Xi, Y. Y. Xu, L. P. Zhu, Y. Wang, and B. K. Zhu, “A facile method of surface modification for hydrophobic polymer membranes based on the adhesive behavior of poly(DOPA) and poly(dopamine),” *Journal of Membrane Science*, vol. 327, no. 1-2, pp. 244-253, Feb. 2009.

[43] F. Bernsmann, O. Ersen, J.-C. Voegel, E. Jan, N. A. Kotov, and V. Ball, “Melanin-containing films: growth from dopamine solutions versus layer-by-layer deposition,” *Chemphyschem : a European journal of chemical physics and physical chemistry*, vol. 48109, pp. 3299-3305, Aug. 2010.

[44] J. Jiang, L. Zhu, X. Li, and Y. Xu, “Surface modification of PE porous membranes based on the strong adhesion of polydopamine and covalent immobilization of heparin,” *Journal of Membrane Science*, vol. 364, no. 1-2, pp. 194-202, 2010.

[45] B. D. McCloskey et al., “Influence of polydopamine deposition conditions on pure water flux and foulant adhesion resistance of reverse osmosis, ultrafiltration, and microfiltration membranes,” *Polymer*, vol. 51, no. 15, pp. 3472-3485, Jul. 2010.

[46] J. Ryu, S. H. Ku, H. Lee, and C. B. Park, “Mussel-inspired polydopamine coating as a universal route to hydroxyapatite crystallization,” *Advanced Functional Materials*, vol. 20, no. 13, pp. 2132–2139, May. 2010.

[47] B. Xing and X. B. Yin, “Novel poly-dopamine adhesive for a halloysite nanotube-Ru(bpy)(3)2+ electrochemiluminescent sensor,” *PloS one*, vol. 4, no. 7, p. e6451, Jan. 2009.

[48] L. Q. Xu, W. J. Yang, K. G. Neoh, E. T. Kang, and G. D. Fu, “Dopamine-induced reduction and functionalization of graphene oxide nanosheets,” *Macromolecules*, vol. 43, no. 20, pp. 8336–8339, Sep. 2010.

[49] M. J. Harrington, A. Masic, N. Holten-Andersen, J. H. Waite, and P. Fratzl, “Iron-clad fibers: a metal-based biological strategy for hard flexible coatings,” *Science (New York, N.Y.)*, vol. 328, no. 5975, pp. 216-20, Apr. 2010.

[50] Q. Wei, F. Zhang, J. Li, B. Li, and C. Zhao, “Oxidant-induced dopamine polymerization for multifunctional coatings,” *Polymer Chemistry*, vol. 1, no. 9, p. 1430, 2010.

[51] P. G. de Gennes, “Wetting: statics and dynamics,” *Reviews of Modern Physics*, vol. 57, no. 3, pp. 827–863, 1985.

[52] J. Beuth Jr, “Cracking of thin bonded films in residual tension,” *International Journal of Solids and Structures*, vol. 29, no. 13, pp. 1657–1675, 1992.

[53] T. Suga, G. Elssner, and S. Schmauder, “Composite parameters and mechanical compatibility of material joints,” *Journal of Composite Materials*, vol. 22, no. 10, pp. 917-934, 1988.

[54] C. N. C. Lam, R. Wu, D. Li, M. L. Hair, and a W. Neumann, “Study of the advancing and receding contact angles: liquid sorption as a cause of contact angle hysteresis,” *Advances in colloid and interface science*, vol. 96, no. 1-3, pp. 169-91, Mar. 2002.

[55] D. N. Moses, M. a Mattoni, N. L. Slack, J. H. Waite, and F. W. Zok, “Role of melanin in mechanical properties of Glycera jaws,” *Acta biomaterialia*, vol. 2, no. 5, pp. 521-30, Sep. 2006.

[56] K. Y. Ju, Y. Lee, S. Lee, S. B. Park, and J. K. Lee, “Bioinspired polymerization of dopamine to generate melanin-like nanoparticles having an excellent free-radical-scavenging property,” *Biomacromolecules*, vol. 12, no. 3, pp. 625-32, Mar. 2011.

[57] P. M. McGuiggan, J. S. Wallace, D. T. Smith, I. Sridhar, Z. W. Zheng, and K. L. Johnson, "Contact mechanics of layered elastic materials: experiment and theory," *Journal of Physics D: Applied Physics*, vol. 40, no. 19, pp. 5984-5994, Oct. 2007.

[58] M. Eriksson, S. M. Notley, and L. Wågberg, "Cellulose thin films: degree of cellulose ordering and its influence on adhesion," *Biomacromolecules*, vol. 8, no. 3, pp. 912-9, Mar. 2007.

[59] M. K. Chaudhury and G. M. Whitesides, "Direct measurement of interfacial interactions between semispherical lenses and flat sheets of poly(dimethylsiloxane) and their chemical derivatives," *Langmuir*, vol. 7, no. 5, pp. 1013-1025, May. 1991.

[60] M. Tirrell, "Measurement of interfacial energy at solid polymer surfaces," *Langmuir*, vol. 12, no. 19, pp. 4548-4551, Jan. 1996.

[61] H. Hertz, "Hertz's miscellaneous papers," *McMillan, London*, vol. 55, no. 1410, pp. 6-9, Nov. 1896.

[62] W. Yang, "The contact problem for viscoelastic bodies," *Journal of Applied Mechanics*, no. 65, 1966.

[63] J. Greenwood and K. Johnson, "A surface roughness parameter in hertz contact," *Wear*, vol. 100, pp. 47 - 57, 1984.

[64] C. Creton and L. Leibler, "How does tack depend on time of contact and contact pressure," *Journal of Polymer Science Part B: Polymer Physics*, vol. 34, no. 3, pp. 545–554, 1996.

[65] K. Johnson, K. Kendall, and A. Roberts, "Surface energy and the contact of elastic solids," *Proceedings of the Royal Society of London. Series A, Mathematical and Physical Sciences*, vol. 324, no. 1558, pp. 301–313, 1971.

[66] K. R. Shull, "Contact mechanics and the adhesion of soft solids," *Materials Science*, vol. 36, pp. 1-45, 2002.

[67] D. Ahn and K. R. Shull, "JKR studies of acrylic elastomer adhesion to glassy polymer substrates," *Macromolecules*, vol. 29, no. 12, pp. 4381–4390, Jan. 1996.

[68] Y. Chen, C. Helm, and J. Israelachvili, “Molecular mechanisms associated with adhesion and contact angle hysteresis of monolayer surfaces,” *The Journal of Physical Chemistry*, vol. 95, no. 26, pp. 10736–10747, 1991.

[69] D. L. Woerdeman, N. Amouroux, V. Ponsinet, G. Jandeau, H. Hervet, and L. Léger, “Characterization of glass-epoxy adhesion using JKR methods and atomic force microscopy,” *Composites Part A: Applied Science and Manufacturing*, vol. 30, no. 1, pp. 95–109, 1999.

[70] F. Podczeck, J. M. Newton, and M. B. James, “The estimation of the true area of contact between microscopic particles and a flat surface in adhesion contact,” *Journal of Applied Physics*, vol. 79, no. 3, p. 1458, 1996.

[71] E. D. Reedy, “Thin-coating contact mechanics with adhesion,” *Journal of Materials Research*, vol. 21, no. 10, pp. 2660-2668, Oct. 2006.

[72] K. Johnson and I. Sridhar, “Adhesion between a spherical indenter and an elastic solid,” *Journal of Physics D: Applied Physics*, vol. 34, pp. 683–689, 2001.

[73] I. Sridhar, Z. W. Zheng, and K. L. Johnson, “A detailed analysis of adhesion mechanics between a compliant elastic coating and a spherical probe,” *Journal of Physics D: Applied Physics*, vol. 37, no. 20, pp. 2886-2895, Oct. 2004.

[74] P. M. McGuiggan, J. S. Wallace, D. T. Smith, I. Sridhar, Z. W. Zheng, and K. L. Johnson, “Contact mechanics of layered elastic materials: experiment and theory,” *Journal of Physics D: Applied Physics*, vol. 40, no. 19, pp. 5984-5994, Oct. 2007.

[75] F. Yang, “Adhesive contact between a rigid axisymmetric indenter and an incompressible elastic thin film,” *Journal of Physics D: Applied Physics*, vol. 35, no. 20, pp. 2614-2620, Oct. 2002.

[76] B. Bhushan, “Springer Handbook of Nanotechnology,” *Ieee Electrical Insulation Magazine*, vol. 21, no. 3, 2010.

[77] F. Streitz, K. Sieradzki, and R. Cammarata, “Elastic properties of thin fcc films,” *Physical Review B*, vol. 41, no. 17 , 1990.

[78] A. M. Kosevich and A. S. Kovalev, “An introduction to nonlinear physical mechanics,” *Kiev Izdatel Naukova Dumka*, vol. 1, 1989.

[79] A. Banerjea and J. R. Smith, “Continuum elasticity analysis of the enhanced modulus effect in metal-alloy superlattice films,” *Physical Review B*, vol. 35, no. 11, p. 5413, 1987.

[80] W. D. Nix and H. Gao, “An atomistic interpretation of interface stress,” *Scripta Materialia(USA)*, vol. 39, no. 12, pp. 1653–1661, 1998.

[81] D. Sander, “Surface stress: implications and measurements,” *Current Opinion in Solid State and Materials Science*, vol. 7, no. 1, pp. 51–57, 2003.

[82] L. M. Kachanov, *Delamination buckling of composite materials*, vol. 14. Springer, 1988, p. 95.

[83] G. Pharr and W. Oliver, “Measurement of thin film mechanical properties using nanoindentation,” *Mrs Bulletin*, vol. 17, no. 7, pp. 28–33, 1992.

[84] R. Saha and W. D. Nix, “Effects of the substrate on the determination of thin film mechanical properties by nanoindentation,” *Acta Materialia*, vol. 50, no. 1, pp. 23–38, 2002.

[85] R. King, “Elastic analysis of some punch problems for a layered medium,” *International Journal of Solids and Structures*, vol. 23, no. 12, pp. 1657–1664, 1987.

[86] M. Dietiker, R. D. Nyilas, C. Solenthaler, and R. Spolenak, “Nanoindentation of single-crystalline gold thin films: Correlating hardness and the onset of plasticity,” *Acta Materialia*, vol. 56, no. 15, pp. 3887-3899, Sep. 2008.

[87] H. Y. Yu, S. C. Sanday, and B. B. Rath, “The effect of substrate on the elastic properties of films determined by the indentation test — axisymmetric boussinesq problem,” *Journal of the Mechanics and Physics of Solids*, vol. 38, no. 6, pp. 745-764, Jan. 1990.

[88] M. Sakai, “Substrate-affected indentation contact parameters of elastoplastic coating/substrate composites,” *Journal of Materials Research*, vol. 24, no. 3, pp. 831-843, Jan. 2009.

[89] H. Li, N. X. Randall, and J. J. Vlassak, "New methods of analyzing indentation experiments on very thin films," *Journal of Materials Research*, vol. 25, no. 4, pp. 728-734, Jan. 2010.

[90] S. Gupta, F. Carrillo, C. Li, L. Pruitt, and C. Puttlitz, "Adhesive forces significantly affect elastic modulus determination of soft polymeric materials in nanoindentation," *Materials Letters*, vol. 61, no. 2, pp. 448-451, Jan. 2007.

[91] K. L. Johnson, *Contact mechanics*. Cambridge University Press, 1987, p. 452.

[92] K. N. G. Fuller and D. Tabor, "The effect of surface roughness on the adhesion of elastic solids," *Proceedings of the Royal Society A: Mathematical, Physical and Engineering Sciences*, vol. 345, no. 1642, pp. 327-342, Sep. 1975.

[93] I. Sridhar, K. Johnson, and N. Fleck, "Adhesion mechanics of the surface force apparatus," *Journal of Physics D: Applied Physics*, vol. 30, p. 1710, 1997.

[94] S. Timoshenko and S. Woinowsky-Krieger, *Theory of Plates and Shells*, vol. 148, no. 3760. McGraw-Hill, 1959.

[95] D. Roylance, *Stress-Strain Curves*. MIT press, 2001.

[96] R. D. Emery and G. L. Povirk, "Tensile behavior of free-standing gold films. Part I. Coarse-grained films," *Acta Materialia*, vol. 51, no. 7, pp. 2067-2078, Apr. 2003.

[97] R. D. Emery and G. L. Povirk, "Tensile behavior of free-standing gold films. Part II. Fine-grained films," *Acta Materialia*, vol. 51, no. 7, pp. 2079-2087, Apr. 2003.

[98] K. Kendall, *Molecular Adhesion and its Applications: the Sticky Universe*. Springer, 2001.

[99] J. Comyn, "The relationship between joint durability and water diffusion," *Developments in adhesives*, 2nd ed. London: Applied Science Publishers, 1981, pp. 279-313.

[100] A. V. Pocius, *Adhesion and adhesives technology: an introduction*. Hanser Verlag, 2002.

[101] W. E. Cloete and W. W. Focke, “Fast underwater bonding to polycarbonate using photoinitiated cyanoacrylate,” *International Journal of Adhesion and Adhesives*, vol. 30, no. 4, pp. 208-213, Jun. 2010.

[102] J. N. Israelachvili, *Intermolecular and Surface Forces: Revised Third Edition*. Academic Press, 2011, p. 704.

[103] V. Gutmann, “Solvent effects on the reactivities of organometallic compounds,” *Coordination Chemistry Reviews*, vol. 18, no. 2, pp. 225-255, 1976.

[104] R. R. Despain, K. L. De Vries, R. D. Luntz, and M. L. Williams, “Comparison of the strength of Barnacle and commercial dental cements,” *Journal of Dental Research*, vol. 52, no. 4, pp. 674-679, Jul. 1973.

[105] A. R. Statz, R. J. Meagher, A. E. Barron, and P. B. Messersmith, “New peptidomimetic polymers for antifouling surfaces,” *Journal of the American Chemical Society*, vol. 127, no. 22, pp. 7972-3, Jun. 2005.

[106] X. Fan, L. Lin, and P. B. Messersmith, “Cell fouling resistance of polymer brushes grafted from Ti substrates by surface-initiated polymerization: effect of ethylene glycol side chain length,” *Biomacromolecules*, vol. 7, no. 8, pp. 2443-8, Aug. 2006.

[107] A. Statz, J. Finlay, J. Dalsin, M. Callow, J. A. Callow, and P. B. Messersmith, “Algal antifouling and fouling-release properties of metal surfaces coated with a polymer inspired by marine mussels,” *Biofouling*, vol. 22, no. 5-6, pp. 391-9, Jan. 2006.

[108] J. L. Dalsin, B.-H. Hu, B. P. Lee, and P. B. Messersmith, “Mussel adhesive protein mimetic polymers for the preparation of nonfouling surfaces,” *Journal of the American Chemical Society*, vol. 125, no. 14, pp. 4253-8, Apr. 2003.

[109] B. P. Lee, J. L. Dalsin, and P. B. Messersmith, “Synthesis and gelation of DOPA-modified poly(ethylene glycol) hydrogels,” *Biomacromolecules*, vol. 3, no. 5, pp. 1038-47, 2002.

[110] C. E. Brubaker, H. Kissler, L.-J. Wang, D. B. Kaufman, and P. B. Messersmith, "Biological performance of mussel-inspired adhesive in extrahepatic islet transplantation," *Biomaterials*, vol. 31, no. 3, pp. 420-7, Jan. 2010.

[111] G. Westwood, T. N. Horton, and J. J. Wilker, "Simplified polymer mimics of cross-linking adhesive proteins," *Macromolecules*, vol. 40, no. 11, pp. 3960-3964, May. 2007.

[112] H. Shao, K. N. Bachus, and R. J. Stewart, "A water-borne adhesive modeled after the sandcastle glue of P. californica," *Macromolecular bioscience*, vol. 9, no. 5, pp. 464-71, May 2009.

[113] H. Shao and R. J. R. J. Stewart, "Biomimetic underwater adhesives with environmentally triggered setting mechanisms," *Advanced materials (Deerfield Beach, Fla.)*, vol. 22, no. 6, pp. 729-33, Feb. 2010.

[114] B. D. Winslow, H. Shao, R. J. Stewart, and P. A. Tresco, "Biocompatibility of adhesive complex coacervates modeled after the sandcastle glue of Phragmatopoma californica for craniofacial reconstruction," *Biomaterials*, vol. 31, no. 36, pp. 9373-81, Dec. 2010.

[115] S. Kaur, G. M. Weerasekare, and R. J. Stewart, "Multiphase adhesive coacervates inspired by the Sandcastle worm," *ACS applied materials & interfaces*, vol. 3, no. 4, pp. 941-4, Apr. 2011.

[116] D. S. Hwang, H. J. Yoo, J. H. Jun, W. K. Moon, and H. J. Cha, "Expression of functional recombinant mussel adhesive protein Mgfp-5 in Escherichia coli," *Applied and environmental microbiology*, vol. 70, no. 6, pp. 3352-9, Jun. 2004.

[117] H. J. Cha, D. S. Hwang, S. Lim, J. D. White, C. R. Matos-Perez, and J. J. Wilker, "Bulk adhesive strength of recombinant hybrid mussel adhesive protein," *Biofouling*, no. 918588849, pp. 1-9, Nov. 2008.

[118] S. Lim, Y. S. Choi, D. G. Kang, Y. H. Song, and H. J. Cha, "The adhesive properties of coacervated recombinant hybrid mussel adhesive proteins," *Biomaterials*, vol. 31, no. 13, pp. 3715-22, May. 2010.

[119] C. J. Van Oss, *Interfacial Forces in Aqueous Media*. CRC, 2006.

[120] E. Arunan et al., "Definition of the hydrogen bond," *Pure and Applied Chemistry*, vol. 83, no. 8, p. 1, Jul. 2011.

[121] R. J. Good, "Contact angle, wetting, and adhesion: a critical review," *Journal of Adhesion Science and Technology*, vol. 6, no. 12, pp. 1269-1302, Jan. 1992.

[122] J. H. Jiang, L. P. Zhu, L. J. Zhu, B.-K. Zhu, and Y. Y. Xu, "Surface Characteristics of Self-polymerized Dopamine Coating Deposited on Hydrophobic Polymer Films," *Langmuir : the ACS journal of surfaces and colloids*, Oct. 2011.

[123] E. Chibowski and L. Holysz, "Use of the Washburn equation for surface free energy determination," *Langmuir*, vol. 8, no. 2, pp. 710–716, 1992.

[124] S. C. Li, J. G. Wang, P. Jacobson, X. Q. Gong, A. Selloni, and U. Diebold, "Correlation between bonding geometry and band gap states at organic-inorganic interfaces: catechol on rutile TiO2(110)," *Journal of the American Chemical Society*, vol. 131, no. 3, pp. 980-4, Jan. 2009.

[125] S. W. Taylor, D. B. Chase, M. H. Emptage, M. J. Nelson, and J. H. Waite, "Ferric ion complexes of a DOPA-containing adhesive protein from Mytilus edulis," *Inorganic Chemistry*, vol. 35, no. 26, pp. 7572-7577, Jan. 1996.

[126] H. Powell and M. Taylor, "Interactions of iron(II) and iron(III) with gallic acid and its homologues: a potentiometric and spectrophotometric study," *Australian Journal of Chemistry*, vol. 35, no. 4, p. 739, 1982.

[127] J. T. Weisser, M. J. Nilges, M. J. Sever, and J. J. Wilker, "EPR investigation and spectral simulations of iron-catecholate complexes and iron-peptide models of marine adhesive cross-links," *Inorganic chemistry*, vol. 45, no. 19, pp. 7736-47, Sep. 2006.

[128] M. J. Sever and J. J. Wilker, "Visible absorption spectra of metal-catecholate and metal-tironate complexes," *Dalton Transactions (Cambridge, England : 2003)*, no. 7, pp. 1061-72, Apr. 2004.

[129] J. J. Wilker, “Marine bioinorganic materials: mussels pumping iron.,” *Current opinion in chemical biology*, vol. 14, no. 2, pp. 276-83, Apr. 2010.

[130] M. J. Sever, J. T. Weisser, J. Monahan, S. Srinivasan, and J. J. Wilker, “Metal-mediated cross-linking in the generation of a marine-mussel adhesive,” *Angewandte Chemie (International ed. in English)*, vol. 43, no. 4, pp. 448-50, Jan. 2004.

[131] T. B. Karpishin, M. S. Gebhard, E. I. Solomon, and K. N. Raymond, “Spectroscopic studies of the electronic structure of iron(III) tris(catecholates),” *Journal of the American Chemical Society*, vol. 113, no. 8, pp. 2977-2984, Apr. 1991.

[132] W. Linert, E. Herlinger, R. F. Jameson, E. Kienzl, K. Jellinger, and M. B. H. Youdim, “Dopamine, 6-hydroxydopamine, iron, and dioxygen - their mutual interactions and possible implication in the development of Parkinson’s disease,” *Biochimica et Biophysica Acta (BBA) - Molecular Basis of Disease*, vol. 1316, no. 3, pp. 160-168, Aug. 1996.

[133] M. J. Harrington, A. Masic, N. Holten-Andersen, J. H. Waite, and P. Fratzl, “Iron-clad fibers: a metal-based biological strategy for hard flexible coatings,” *Science (New York, N.Y.)*, vol. 328, no. 5975, pp. 216-20, Apr. 2010.

[134] D. S. Hwang, H. Zeng, A. Masic, M. J. Harrington, J. N. Israelachvili, and J. H. Waite, “Protein- and metal-dependent interactions of a prominent protein in mussel adhesive plaques,” *The Journal of biological chemistry*, vol. 285, no. 33, pp. 25850-8, Aug. 2010

[135] H. Zeng, D. S. Hwang, J. N. Israelachvili, and J. H. Waite, “Strong reversible Fe3+-mediated bridging between dopa-containing protein films in water,” *Proceedings of the National Academy of Sciences of the United States of America*, vol. 107, no. 29, pp. 12850-3, Jul. 2010.

[136] N. Holten-Andersen, M.J. Harrington, H. Birkedal, B.P. Lee, P.B. Messersmith, K.Y.C. Lee, and J.H. Waite, “pH-induced metal-ligand cross-links inspired by mussel yield self-healing polymer networks with near-covalent elastic modulus.,” *Proceedings of the National Academy of Sciences of the United States of America*, vol. 5, Jan. 2011, pp. 3-7.

[137] Y. Dong, W. Dong, Y. Cao, Z. Han, and Z. Ding, “Preparation and catalytic activity of Fe alginate gel beads for oxidative degradation of azo dyes under visible light irradiation,” *Catalysis Today*, Apr. 2011.

[138] J. Burkett, J. Wojtas, J. Cloud, and J. Wilker, “A method for measuring the adhesion strength of marine mussels,” *The Journal of Adhesion*, vol. 85, no. 9, pp. 601-615, Sep. 2009.

[139] D. S. Hwang et al., “Viscosity and interfacial properties in a mussel-inspired adhesive coacervate,” *Soft Matter*, vol. 6, no. 14, p. 3232, 2010.